Article

Cell Host & Microbe

Gut microbiota and metabolites drive chronic sickle cell disease pain in mice

Graphical abstract

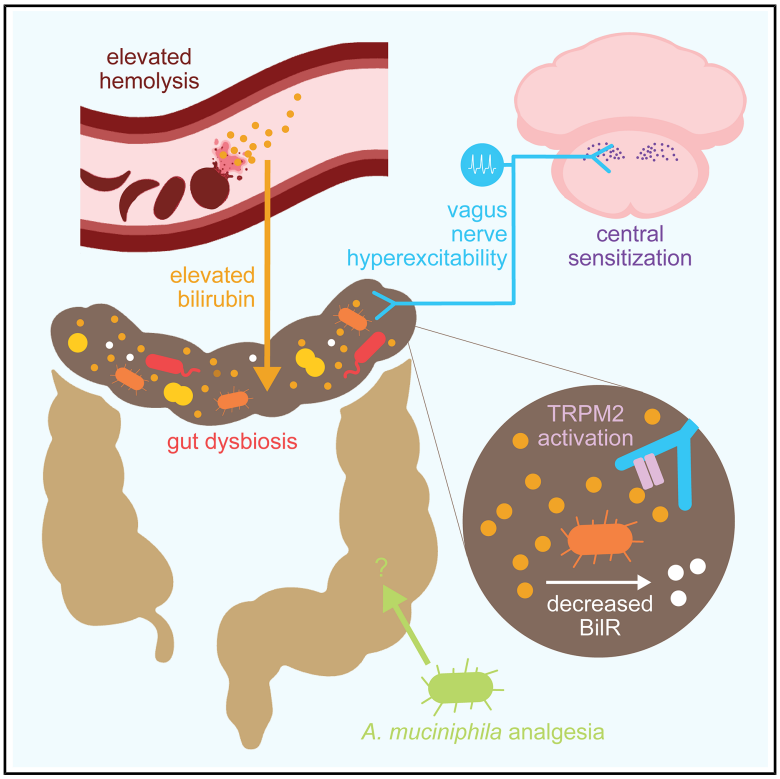

Highlights

- Sickle cell mice exhibit gut dysbiosis and high levels of heme catabolites in feces
- *Akkermansia muciniphila* decreases pain in transgenic sickle cell disease mice
- Elevated intestinal bilirubin drives pain by activating TRPM2 on vagal afferents
- BilR-expressing bacteria are decreased in sickle cell patient gut

Authors

Amanda M. Brandow, Samantha N. Atkinson, Zulmary Manjarres, ..., Cheryl L. Stucky, Theodore J. Price, Katelyn E. Sadler

Correspondence

katelyn.sadler@utdallas.edu

In brief

Brandow et al. describe how the gut microbiome drives chronic sickle cell disease (SCD) pain. SCD guts contain excessive heme catabolites, fewer bacteria that metabolize bilirubin, and low levels of *Akkermansia muciniphila*. Addition of *A. muciniphila* or treatment with TRPM2 inhibitors—which block bilirubin-induced vagus nerve activity—alleviate SCD pain.

Brandow et al., 2025, Cell Host & Microbe *33*, 1–12
October 8, 2025
https://doi.org/10.1016/j.chom.2025.08.012

CellPress

Please cite this article in press as: Brandow et al., Gut microbiota and metabolites drive chronic sickle cell disease pain in mice, Cell Host & Microbe (2025), https://doi.org/10.1016/j.chom.2025.08.012

Cell Host & Microbe

CellPress

Article

Gut microbiota and metabolites drive chronic sickle cell disease pain in mice

Amanda M. Brandow,[1] Samantha N. Atkinson,[2,3] Zulmary Manjarres,[5,6] Vanessa L. Ehlers,[4] McKenna L. Pratt,[5,6] Iti Mehta,[7] Sruthi Mudunuri,[7] Aishwarya Kappagantu,[7] Stephanie I. Shiers,[5,6] Khadijah Mazhar,[5,6] Mackenzie A. Simms,[5,6,7] Sahar Alhendi,[7] Anagha Sheshadri,[7] Anna M. Cervantes,[8] Jeffrey C. Reese,[8] Diana Tavares-Ferreira,[5,6] Ishwarya Sankaranarayanan,[5,6] Mandee K. Schaub,[5,6] Tyler B. Waltz,[4] Michael Hayward,[2,9] Dianise M. Rodríguez García,[4] Gregory Dussor,[5,6] Nita H. Salzman,[2,3,9] Kelli L. Palmer,[7] Cheryl L. Stucky,[4] Theodore J. Price,[5,6] and Katelyn E. Sadler[5,6,10,*]

[1]Department of Pediatrics, Division of Hematology/Oncology, Bone Marrow Transplantation, Medical College of Wisconsin, Milwaukee, WI 53226, USA
[2]Center for Microbiome Research, Medical College of Wisconsin, Milwaukee, WI 53226, USA
[3]Department of Microbiology and Immunology, Medical College of Wisconsin, Milwaukee, WI 53226, USA
[4]Department of Cell Biology, Neurobiology & Anatomy, Medical College of Wisconsin, Milwaukee, WI 53226, USA
[5]Department of Neuroscience, The University of Texas at Dallas, Richardson, TX 75080, USA
[6]Center for Advanced Pain Studies, The University of Texas at Dallas, Richardson, TX 75080, USA
[7]Department of Biological Sciences, The University of Texas at Dallas, Richardson, TX 75080, USA
[8]Southwest Transplant Alliance, Dallas, TX 75231, USA
[9]Department of Pediatrics, Division of Gastroenterology, Medical College of Wisconsin, Milwaukee, WI 53226, USA
[10]Lead contact
*Correspondence: katelyn.sadler@utdallas.edu
https://doi.org/10.1016/j.chom.2025.08.012

SUMMARY

Individuals with sickle cell disease (SCD) suffer from debilitating chronic pain that does not have a clear etiology. Recent 16S ribosomal RNA gene sequencing studies revealed gut dysbiosis in individuals with SCD. It is unclear, however, whether these intestinal microbial changes contribute to chronic SCD pain. Using transgenic SCD mice, we determined that chronic SCD pain is alleviated following fecal microbiota transplantation from healthy controls, specifically by increasing the relative abundance of probiotic *Akkermansia muciniphila*. Reciprocally, transplantation of the SCD gut microbiome induced persistent pain in wild-type recipients via bilirubin-vagus nerve TRPM2 signaling. Biospecimens from individuals with SCD and spatial transcriptomic analysis of human nodose ganglia tissue identified additional bacterial species and neuronally expressed transcripts that should be explored as novel SCD analgesic targets.

INTRODUCTION

Individuals with sickle cell disease (SCD), the most common genetic blood disorder in the world, live with widespread chronic pain. Because the biological basis of sickle cell pain is poorly understood, few effective non-opioid-based treatment options exist to manage this symptom. Curative therapies, including hematopoietic stem cell transplant, decrease chronic pain reports in patients,[1] thus suggesting that ongoing red blood cell sickling, vaso-occlusion, tissue hypoxia, and hemolysis promote chronic SCD pain. Given that these processes and their inflammatory metabolic products converge at the gastrointestinal tract, we hypothesized that chronic SCD pain may be driven by disruption of the environment in which gut bacteria reside. In support of this idea, recent 16S rRNA gene sequencing studies revealed differences in the number and types of bacteria found in stool collected from patients with SCD relative to healthy, age-, race-, and gender-matched controls.[2,3] However, it is unclear whether this gut dysbiosis contributes to chronic SCD pain or is simply a result of underlying disease pathology. Here, we used transgenic SCD mice, patient biospecimens, and human peripheral nervous system tissue to determine the extent to and mechanisms through which the gut microbiome contributes to chronic SCD pain.

RESULTS

Chronic SCD pain is alleviated by *Akkermansia muciniphila*

To begin, 16S rRNA gene sequencing was performed on fecal material collected from mice expressing normal (hemoglobin AA [HbAA], control) or sickle (hemoglobin SS [HbSS], SCD) human β-globin.[4] Bacterial populations in SCD mouse feces were more diverse (Figure 1A) and distinct from those found in hemoglobin control feces (Figure 1B). Next, a series of fecal microbiota transplant (FMT) experiments was performed to determine if the chronic pain exhibited by SCD mice could be alleviated via replacement of their gut contents with the gastrointestinal

Please cite this article in press as: Brandow et al., Gut microbiota and metabolites drive chronic sickle cell disease pain in mice, Cell Host & Microbe (2025), https://doi.org/10.1016/j.chom.2025.08.012

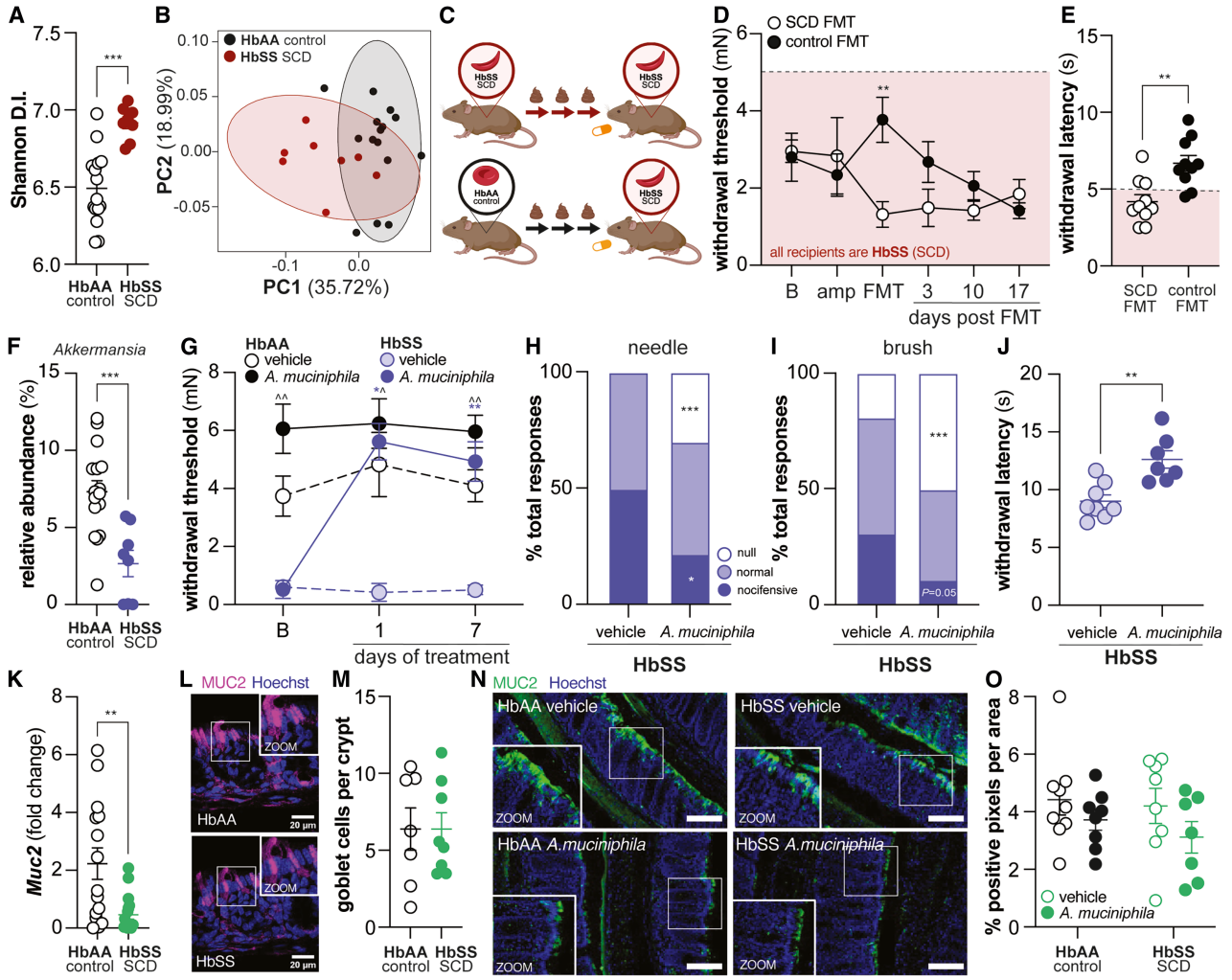

Figure 1. Chronic SCD pain is reversed via FMT or *Akkermansia muciniphila* probiotic treatment

(A) Alpha diversity of fecal samples collected from Townes HbAA (control) and HbSS (SCD) mice.

(B) Principal coordinate analysis plot of weighted UniFrac beta diversity measure of Townes HbSS and HbAA feces.

(C) 3-day FMT paradigm design for antibiotic pre-treated SCD mice.

(D) Hindpaw mechanical withdrawal thresholds of SCD mice during the FMT paradigm. The dashed line indicates the average withdrawal threshold of HbAA control mice. B, baseline; amp, ampicillin treatment day 3 of 7, $n = 9–10$.

(E) Hindpaw withdrawal latency of SCD mice to dry ice application at the FMT time point. The dashed line indicates average withdrawal latency of HbAA control mice; unpaired t test, $^{**}p < 0.01$.

(F) Relative abundance of genus *Akkermansia* in Townes HbAA and HbSS feces; unpaired t test, $^{***}p < 0.0001$.

(G) Hindpaw mechanical withdrawal thresholds of control (HbAA) and SCD (HbSS) mice prior to and during *A. muciniphila* supplementation; AA vehicle vs. SS vehicle, $^{\wedge\wedge}p < 0.01$, $^{\wedge}p < 0.05$; SS vehicle vs. SS *A. muciniphila*, $^{*}p < 0.05$, $^{**}p < 0.01$; B, baseline; $n = 7–8$.

(H–J) SCD mouse responses to hindpaw (H) needle; Fisher's exact test, $^{*}p < 0.05$, $^{***}p < 0.001$; (I) brush; Fisher's exact test, $^{***}p < 0.001$; and (J) dry ice stimulation following 7 days of *A. muciniphila* treatment; Mann-Whitney test, $^{**}p < 0.01$.

(K) Relative *Muc2* fold change as assessed by qPCR in distal colon of control and SCD mice; unpaired t test, $^{**}p < 0.01$.

(L) Representative images of MUC2+ goblet cells (magenta) and Hoechst (violet) from the colon of SCD and control mice.

(M) MUC2+ goblet cell quantification.

(N) Representative images of MUC2 (green) and Hoechst (violet) from the colon of SCD and control mice following 7 days of vehicle or *A. muciniphila* treatment.

(O) MUC2+ quantification.

contents of healthy hemoglobin control mice (Figure 1C). SCD mice that received hemoglobin control FMT exhibited a transient, partial reversal of mechanical allodynia (Figure 1D) and cold hypersensitivity (Figure 1E) relative to mice that received FMT from a separate cohort of SCD mice. Based on these data, we concluded that healthy hemoglobin control fecal material contained bacteria or metabolites with analgesic properties, such that when introduced to the SCD gastrointestinal tract, persistent pain in SCD mice was alleviated. Bacteria from several genera were present at different levels in SCD and hemoglobin control feces (Figure S1). Most notably, bacteria from the genus *Akkermansia* were less abundant in SCD mouse feces

Please cite this article in press as: Brandow et al., Gut microbiota and metabolites drive chronic sickle cell disease pain in mice, Cell Host & Microbe (2025), https://doi.org/10.1016/j.chom.2025.08.012

(Figure 1F), mirroring results obtained from individuals with SCD.[2] *Akkermansia muciniphila* has recently gained attention as a promising next-generation probiotic due to its beneficial effects on gut epithelium integrity and ability to produce anti-inflammatory short-chain fatty acids (SCFAs).[5] Thus, to determine if *A. muciniphila* supplementation alleviates chronic SCD pain, mechanical and cold hypersensitivity were measured in SCD mice prior to and during diet supplementation with commercially available *A. muciniphila* (Figures S2A and S2B). Administration of live *A. muciniphila* decreased the punctate mechanical allodynia (Figure 1G), mechanical hyperalgesia (Figure 1H), dynamic mechanical hypersensitivity (Figure 1I), and cold hypersensitivity (Figure 1J) observed in SCD mice. Notably, administration of freeze-dried *A. muciniphila* directly from the commercial capsules also alleviated mechanical and cold hypersensitivity in SCD mice (Figures S2C and S2D).

To characterize the mechanism of *Akkermansia* analgesia in SCD, we began by examining organs with known SCD pathology. Administration of neither live nor freeze-dried *A. muciniphila* reversed SCD splenomegaly (Figures S2E and S2F), but live *A. muciniphila* treatment did decrease the enlarged cecum observed in SCD mice (Figures S2G and S2H). Given this change in cecum size and the fact that *Akkermansia* is capable of fermenting fiber into SCFAs,[6] we hypothesized that *A. muciniphila* treatment altered production of these anti-inflammatory compounds in SCD mice. Although vehicle-treated SCD mice were indeed found to have decreased butyrate and acetate in their feces, *A. muciniphila* treatment did not reverse this phenotype or change SCFA concentrations in hemoglobin control mouse feces (Figures S2I–S2P). We next reasoned that *A. muciniphila* analgesia may result from repair of gut barrier integrity, a known pathology in both patients[7] and mice with SCD.[8–10] To this end, we measured the relative expression of tight junction gene transcripts in the distal colon of SCD mice and hemoglobin control animals. *A. muciniphila* treatment did not change levels of *Ocln* or *Cldn2*, the genes for occludin and claudin-2, respectively, in either SCD or hemoglobin control colons (Figures S2Q and S2R). Tight junction protein expression is one of only several factors that influences intestinal permeability, however. Decreased goblet cell production of mucus may also increase intestinal epithelium vulnerability, ultimately leading to gut leakiness. Notably, decreased expression of *Muc2*, the gene that encodes critical mucus protein mucin 2, was reported in SCD colons (Figure 1K) despite similar goblet cell density in SCD and hemoglobin control colonic crypts (Figures 1L and 1M). MUC2 protein levels in the distal colon of SCD mice did not differ from hemoglobin control mice, however, regardless of *A. muciniphila* supplementation (Figures 1N and 1O). Divergent *Muc2* RNA and MUC2 protein levels in vehicle-treated SCD mice and hemoglobin controls likely result from the decreased abundance of microbes that use mucin as a primary food source in the SCD colon. Thus, in summary, chronic SCD pain was alleviated by increasing levels of *A. muciniphila* in the gut, a bacterium that is found in critically low levels in both patients[2] and mice with SCD. Exogenous introduction of this bacterium did not change SCFA levels in feces, tight junction protein expression, or mucus production in SCD mice, therefore implying that *A. muciniphila* analgesia results from a previously undescribed mechanism.

SCD gut contents drive persistent pain by altering vagal afferent excitability

We next sought to assess the extent to which the SCD microbiome induces pain in the absence of additional sickle cell pathology. To this end, naive C57BL/6 mice received FMT once per day for 3 days from either SCD or hemoglobin control mice (Figure 2A). C57BL/6 mice that received SCD FMT developed mechanical allodynia that persisted for at least 2 weeks, whereas hemoglobin control FMT recipients demonstrated no change in mechanical sensitivity (Figure 2B). SCD FMT recipients also developed cold allodynia (Figure 2C) like that observed in patients and mouse models with this condition[11,12] and ongoing pain as assessed by facial grimace (Figure 2D). Confirmation of the FMT phenotypes was completed in antibiotic pre-treated C57BL/6 mice (Figures S3A and S3B). Antibiotic-pre-treated SCD FMT recipients developed mechanical allodynia, cold hypersensitivity, mechanical hyperalgesia, dynamic mechanical hypersensitivity, and—in male SCD FMT recipients specifically—heat hypersensitivity (Figures S3C–S3H) that mirrored phenotypes observed in naive SCD FMT recipients.

To begin to investigate the mechanisms through which SCD gastrointestinal cues ultimately influence pain behaviors, we first examined gut epithelium integrity in FMT recipients, as gut leakiness may promote local inflammation and ultimately lead to sensitization of extrinsic sensory afferents. No difference was observed between SCD and control FMT recipients in gut permeability as measured by either fluorescein isothiocyanate (FITC)-dextran serum levels (Figure S3I) or bacterial translocation (Figure S3J). We next performed whole-cell patch clamp recordings on nodose ganglia neurons isolated from FMT recipients to determine if SCD FMT increased ascending sensory transmission from the gut. Two subtypes of nodose jugular ganglion (NJG; one structure in mouse) neurons were observed during recordings: neurons that fired only once upon sustained depolarization (1×; single-fire) and neurons that fired repeatedly (>1×; multiple-fire) during prolonged current injection. Although FMT donor genotype had no effect on single-fire neuron resting or active membrane properties (Table S1), increased excitability was observed in multiple-fire neurons isolated from animals that received SCD FMT (Figures 2E and 2F). Neurons isolated from SCD FMT recipients fired more action potentials upon depolarization than neurons from hemoglobin control FMT recipients. Vagus nerve signaling requirements for chronic SCD pain were further confirmed in SCD mice; SCD mice that received bilateral subdiaphragmatic vagotomy exhibited a complete reversal of punctate mechanical allodynia and a partial reversal of dynamic mechanical allodynia while maintaining mechanical hyperalgesia levels (Figures 2G–2I). Thus, based on these results, SCD gastrointestinal contents drive chronic SCD pain by increasing activity of vagal afferents.

After observing FMT-related increases in NJG neuronal excitability and decreased pain in SCD mice after vagotomy, we next profiled the contents of both SCD and hemoglobin control guts to identify factors that could be acting on nerve terminals and ultimately inducing peripheral neuron sensitization. We first performed 16S rRNA gene sequencing on feces collected from SCD and hemoglobin control FMT recipients prior to and 24 h following the last FMT. Overall, antibiotic microbiome depletion and subsequent FMT decreased microbial diversity to a similar

Please cite this article in press as: Brandow et al., Gut microbiota and metabolites drive chronic sickle cell disease pain in mice, Cell Host & Microbe (2025), https://doi.org/10.1016/j.chom.2025.08.012

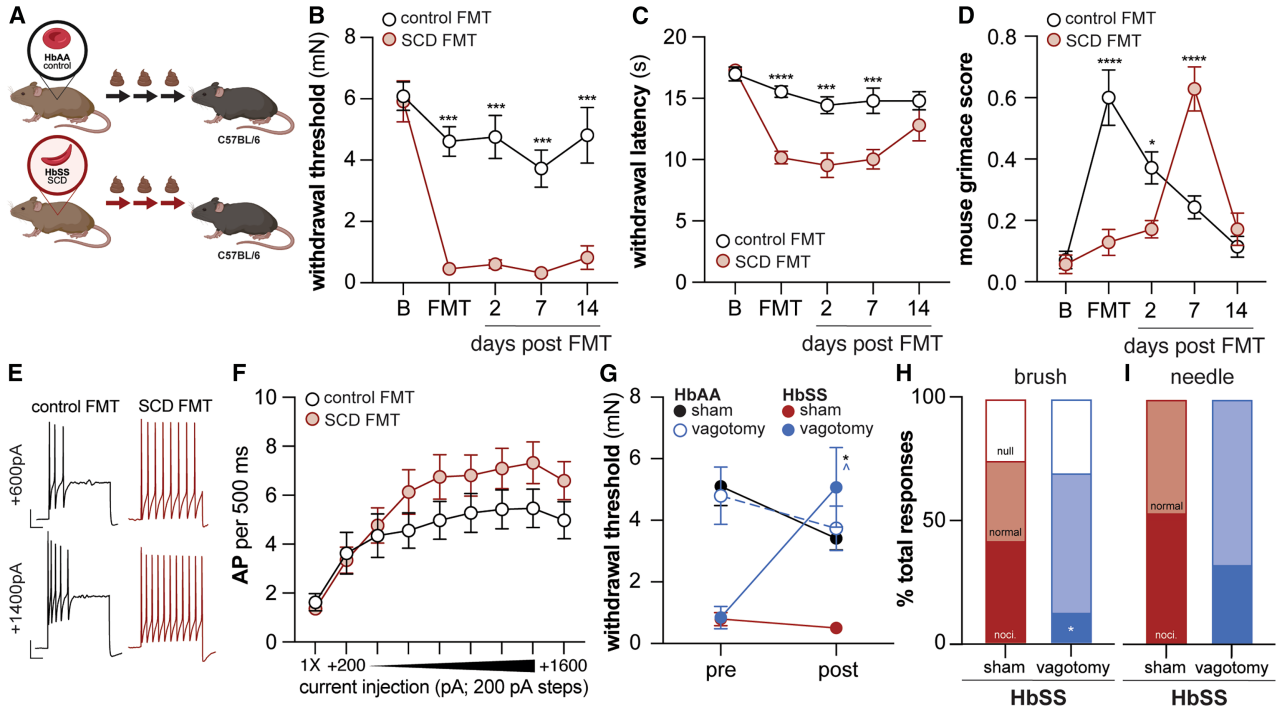

Figure 2. SCD intestinal contents drive persistent pain in a vagus nerve-dependent fashion

(A) 3-day FMT paradigm design for C57BL/6 mice.

(B and C) Hindpaw (B) mechanical withdrawal thresholds and (C) cold withdrawal latencies of C57BL/6 mice during the FMT paradigm. B, baseline; $n = 10$.

(D) Facial grimace score of C57BL/6 mice during FMT paradigm; $n = 10$.

(E) Representative activity from NJG neurons.

(F) Spikes fired by NJG neurons during stepwise increasing pulses of depolarizing current; 1×: rheobase, $n = 39–52$ total neurons isolated from 11 control or SCD FMT recipients at FMT time point.

(G) Hindpaw mechanical withdrawal thresholds of HbAA (control) and HbSS (SCD) mice prior to and following bilateral subdiaphragmatic vagotomy; $n = 5–6$.

(H and I) SCD mouse responses to hindpaw (H) brush; Fisher's exact test, $^*p < 0.05$; and (I) needle stimulation following sham or vagotomy surgery; $n = 5–6$; noci., nocifensive. Unless otherwise noted, Bonferroni post hoc comparison: $^*p < 0.05$, $^{***}p < 0.001$, and $^{****}p < 0.0001$.

extent in both SCD and hemoglobin control FMT recipients (Figures 3A and 3B). Following FMT, feces from SCD and hemoglobin control FMT recipients contained similar bacterial populations (Figure 3C red vs. white circles). Only two bacterial genera—*Enterorhabdus* and *Roseburia*—were differentially abundant between treatment groups (Figures S3K and S3L). Based on these analyses, it is likely that the genotype-specific, FMT-related change in vagus nerve excitability does not result from the establishment of genetically diverse bacterial populations, at least not immediately following FMT.

Considering the lack of change in bacterial populations between hemoglobin control and SCD FMT recipients, we next hypothesized that FMT donor host or bacterial metabolites may be responsible for FMT-related increases in NJG neuronal excitability and pain behaviors. To this end, unbiased metabolomic screening was performed on SCD and hemoglobin control mouse donor feces as well as SCD and hemoglobin control FMT recipient feces (Figure 3E). Of the >2,000 compounds identified across samples, heme catabolism products were among the most dysregulated biochemicals (Figure 3D). Biliverdin (Figure 3F) and isomeric forms of bilirubin (Figures 3G and 3H), two initial heme breakdown products, were elevated in fecal material from SCD mice relative to feces collected from hemoglobin control animals, control FMT recipients, and SCD FMT recipients. Urobilinogen, a compound generated when gut bacteria catabolize bilirubin, was also elevated in SCD fecal material relative to hemoglobin control feces and was only detected in one SCD FMT recipient sample (Figure 3I). Similar observations were also noted for urobilin (Figure 3J). Thus, heme breakdown products may be the primary gastrointestinal metabolites that drive pain following SCD FMT.

Gastrointestinal bilirubin signaling through TRPM2 drives SCD pain

Since bilirubin is directly catabolized by gut bacteria,[13] we hypothesized that this compound may be the critical component of the sickle cell microbiome that induces persistent pain and alters sensory neuron activity following FMT. To directly test this hypothesis, we performed another set of FMT experiments that involved transplant of feces collected from either naive SCD mice or SCD mice that had been maintained on hydroxyurea (HU) treatment since birth. HU is a lifelong, standard-of-care, disease-modifying treatment for individuals with SCD due to its ability to increase fetal hemoglobin levels.[14] Fetal hemoglobin cannot polymerize like diseased adult hemoglobin, and thus patients who are maintained on HU have marked improvement in

Please cite this article in press as: Brandow et al., Gut microbiota and metabolites drive chronic sickle cell disease pain in mice, Cell Host & Microbe (2025), https://doi.org/10.1016/j.chom.2025.08.012

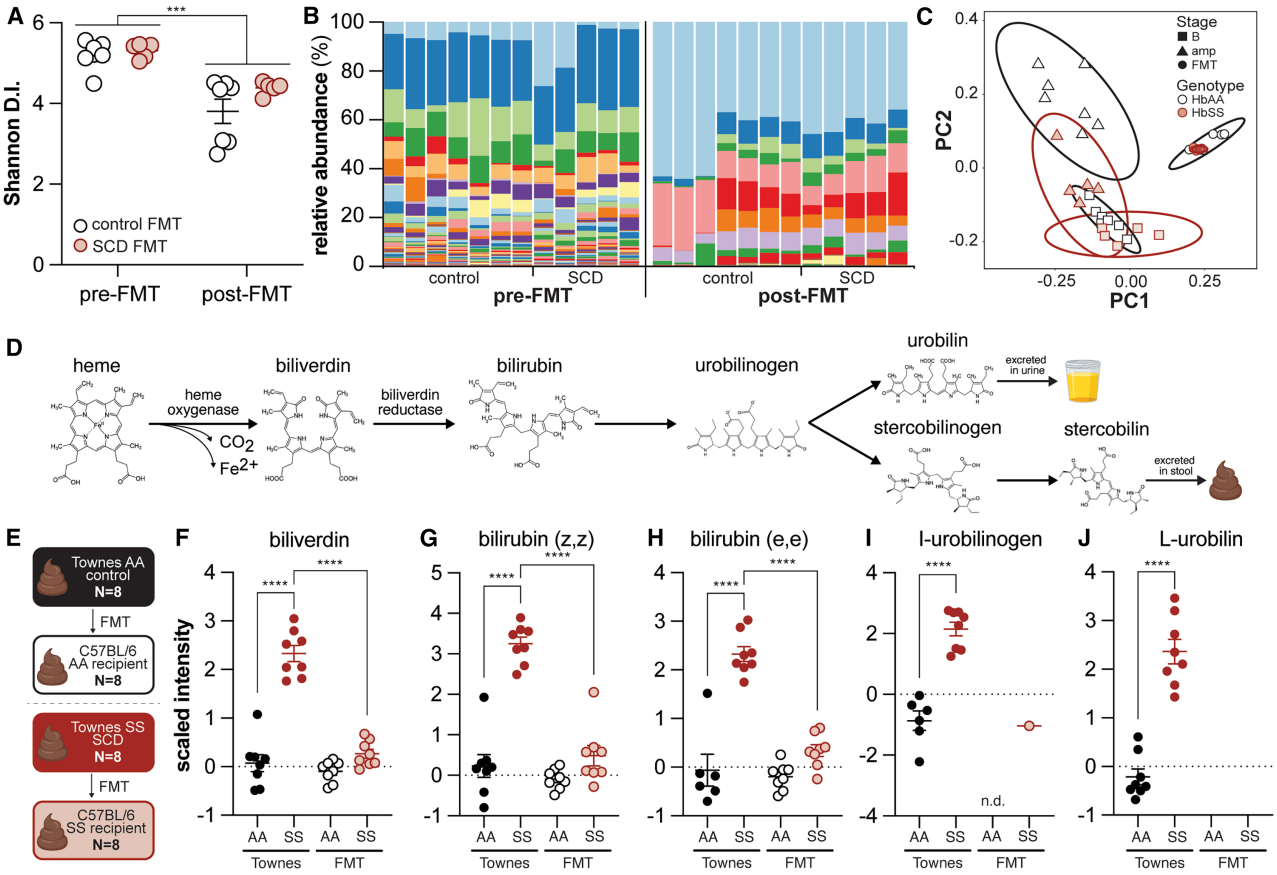

Figure 3. Bacterial and metabolic changes detected in feces following SCD FMT

(A) Alpha diversity of fecal samples collected from C57BL/6 mice prior to and following FMT; two-way ANOVA overall effect of stage, ***$p < 0.001$.

(B) Relative abundance of bacterial genera detected in fecal samples collected from C57BL/6 mice prior to and following FMT.

(C) Principal coordinate analysis plot of weighted UniFrac beta diversity measures of FMT recipient feces at various points in the paradigm.

(D) Heme catabolism pathway.

(E) Subjects from which fecal samples were collected for metabolomic analysis.

(F–J) Relative levels of (F) biliverdin, (G) bilirubin (z,z), (H) bilirubin (e,e), (I) I-urobilinogen, and (J) L-urobilin in fecal samples collected from control (AA) and SCD (SS) FMT donors (Townes) and recipients. Unless otherwise noted, Bonferroni post hoc comparison: ****$p < 0.0001$.

many hematological parameters, including decreased circulating bilirubin due to reduced hemolysis[15] (Figure 4A). Similar to reported observations in plasma,[15] bilirubin levels were decreased in fecal material collected from HU-treated SCD mice (Figure 4B). Unlike the effects of naive SCD FMT, transplant of fecal material from HU-treated SCD mice did not induce mechanical allodynia in naive recipients (Figure 4C). Based on these data, therapies targeted at reducing gastrointestinal bilirubin signaling may prove effective in treating chronic SCD pain.

To determine the mechanisms through which elevated intestinal bilirubin drives chronic SCD pain, we performed a series of experiments in wild-type animals. First, 16S rRNA gene sequencing was performed on fecal material collected from SCD mice and hemoglobin control animals prior to, 24 h following, and 5 days following oral bilirubin administration to determine if elevated gastrointestinal bilirubin induces pain by shifting the gut microbiome to more closely resemble that of SCD mice. Bacterial populations in SCD feces were more diverse than those detected in hemoglobin control samples collected before or after bilirubin treatment (Figure S4A), and although bacterial populations changed in hemoglobin control animals following bilirubin administration, they remained distinct from those observed in SCD fecal material (Figure S4B). These results suggest that microbial populations in the SCD mouse gut result from additional selective pressures, not just elevated bilirubin.

Next, bilirubin was orally administered to wild-type mice, and pain-like behaviors were assessed 30 min later to determine if acute bilirubin exposure induces intestinal nociceptive signaling. Indeed, bilirubin-treated mice exhibited dose-dependent, hindpaw mechanical allodynia 30 min following oral administration, suggesting immediate nociceptive properties of this compound (Figure 4D). Similar to results obtained following SCD FMT, oral bilirubin administration also increased the excitability of multiple-fire NJG neurons (Figures 4E and 4F). Bilirubin administration did not alter resting or active membrane properties of single-fire NJG neurons (Table S2). Given this bilirubin-induced hyperexcitability of NJG neurons, we also examined

Please cite this article in press as: Brandow et al., Gut microbiota and metabolites drive chronic sickle cell disease pain in mice, Cell Host & Microbe (2025), https://doi.org/10.1016/j.chom.2025.08.012

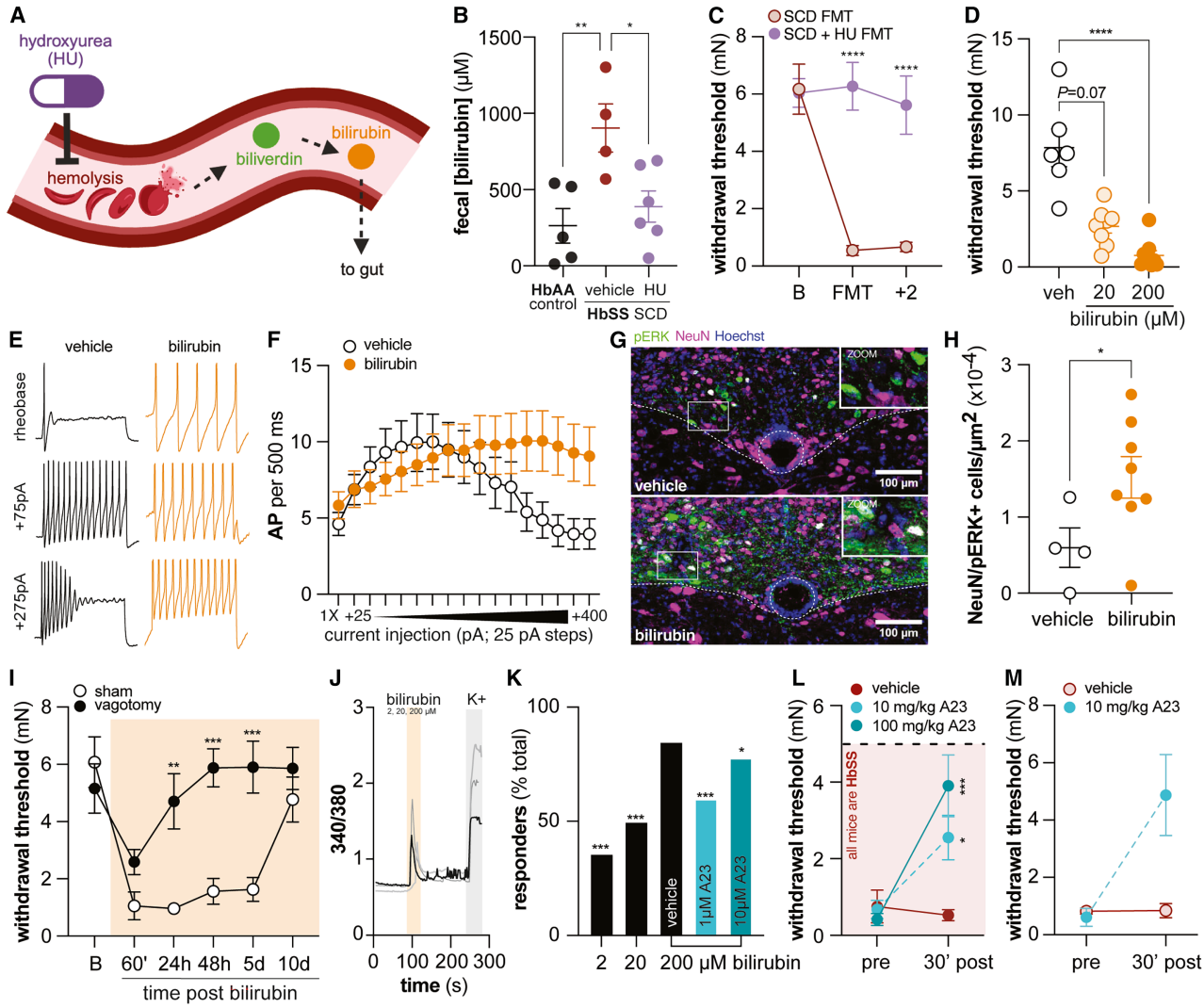

Figure 4. SCD FMT-related pain is driven by bilirubin signaling through vagal TRPM2

(A) Hemolysis-associated heme catabolism in SCD.

(B) Bilirubin concentration in fecal samples collected from HbAA (control), vehicle-, and HU-treated HbSS (SCD) mice.

(C) Hindpaw mechanical withdrawal thresholds of C57BL/6 mice during FMT. B, baseline; +2, 2 days post-last FMT; n = 9–10.

(D) Hindpaw mechanical withdrawal thresholds of HbAA control mice 30 min following oral administration of bilirubin or vehicle.

(E) Representative activity from NJG neurons.

(F) Spikes fired by NJG neurons during stepwise increasing pulses of depolarizing current; 1×: rheobase, n = 18–23 total neurons isolated from 7 to 8 mice 24 h following oral vehicle or 200 μM bilirubin treatment.

(G) Representative images of the NTS stained for pERK1/2 (green), NeuN (magenta), and Hoechst (violet).

(H) pERK1/2 and NeuN co-localization quantification in NTS.

(I) Hindpaw mechanical withdrawal thresholds of hemoglobin control mice with intact (sham) or transected (vagotomy) vagus nerve following oral bilirubin (200 μM) administration; n = 8–9.

(J) Example calcium flux in NJG neurons exposed to a 30-s pulse of bilirubin (2, 20, or 200 μM) then 50-mM KCl.

(K) Quantification of NJG neurons that exhibited response to varying bilirubin concentrations or 200 μM bilirubin application in conjunction with TRPM2 inhibitor A23 (2 min A23 incubation prior to bilirubin application); n = 90–338 neurons from 4 to 6 C57BL/6 mice.

(L) Hindpaw mechanical withdrawal thresholds of HbSS (SCD) mice prior to or 30 min following oral administration of A23; n = 8.

(M) Hindpaw mechanical withdrawal thresholds of SCD FMT recipients prior to or 30 min following oral administration of A23; n = 7. Bonferroni post hoc comparisons: $^{*}p < 0.05$, $^{**}p < 0.01$, $^{***}p < 0.001$, and $^{****}p < 0.0001$.

phosphorylated extracellular signal-regulated kinase 1/2 (pERK1/2) expression[16] in the nucleus of the solitary tract (NTS)—the primary termination site of vagal afferents—from vehicle- and bilirubin-treated mice (Figure 4G). Increased pERK1/2 expression was observed in NTS neurons of bilirubin-treated mice, supporting the idea that altered intestinal chemosensation can promote central sensitization (Figure 4H). Finally, to definitively determine if vagus nerve signaling is required for

Please cite this article in press as: Brandow et al., Gut microbiota and metabolites drive chronic sickle cell disease pain in mice, Cell Host & Microbe (2025), https://doi.org/10.1016/j.chom.2025.08.012

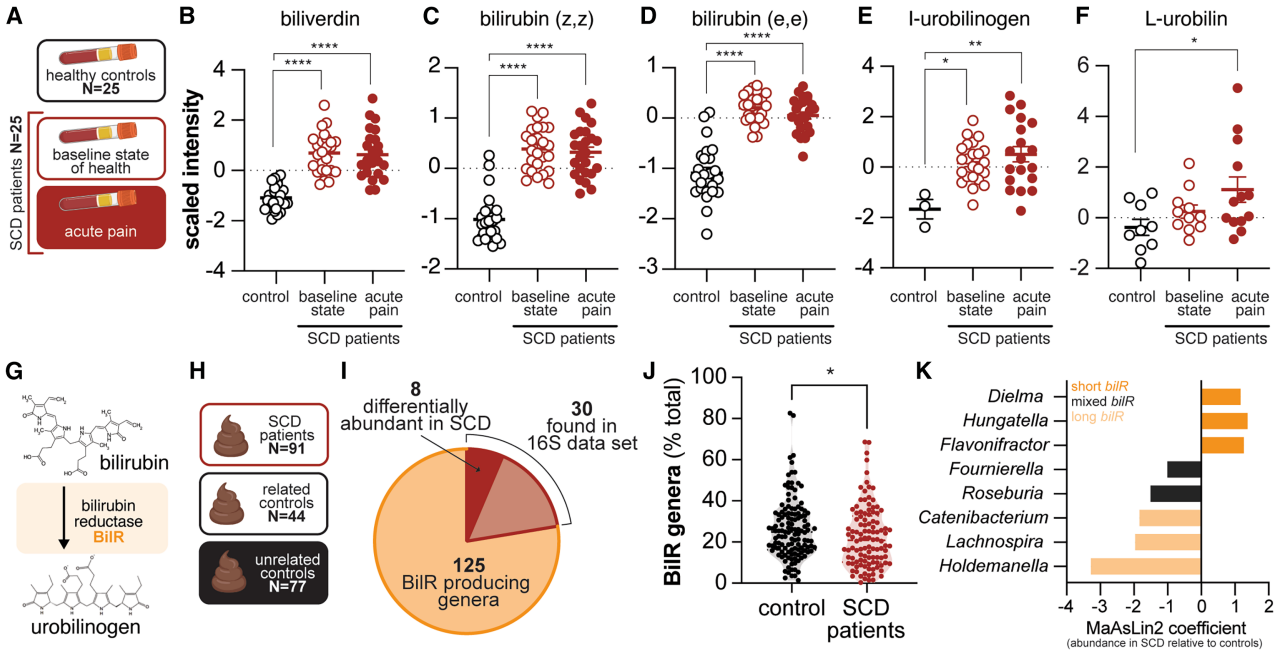

Figure 5. Altered bilirubin catabolism in individuals with SCD

(A) Individuals from whom plasma was collected for metabolomic analysis.

(B–F) Relative levels of (B) biliverdin, (C) bilirubin (z,z), (D) bilirubin (e,e), (E) I-urobilinogen, and (F) L-urobilin in plasma from healthy controls and individuals with SCD during both baseline state of health and acute pain.

(G) Bacterially expressed BilR catabolizes bilirubin into urobilinogen.

(H) Individuals from whom stool was collected for 16S sequencing.

(I) Summary of BilR-expressing bacteria identified in the current experiment.

(J) Relative abundance of total BilR-expressing genera in stool samples collected from healthy controls and individuals with SCD.

(K) Relative change in abundance of genera that express the long or short form of *bilR* in stool collected from individuals with SCD. Bonferroni post hoc comparisons: $*p < 0.05$, $**p < 0.01$, and $****p < 0.0001$.

intestinal bilirubin-related pain, hindpaw mechanical sensitivity was measured in sham mice or mice that underwent subdiaphragmatic vagotomy several days prior to oral bilirubin administration. Vagotomized mice developed immediate bilirubin-induced hypersensitivity but did not exhibit persistent bilirubin-related mechanical allodynia like that observed in sham control mice (Figure 4I). Collectively, these data support the idea that elevated levels of bilirubin in the gastrointestinal tract—like that observed in SCD mice—drive vagus nerve hyperexcitability and subsequent central sensitization.

In an effort to identify the molecular target of bilirubin in vagal afferents, we next used *in vitro* calcium imaging to measure bilirubin-induced NJG neuronal activity. Acute extracellular application of bilirubininduced calcium flux in wild-type mouse NJG neurons in a concentration-dependent fashion (Figures 4J and 4K). Almost immediately following extracellular application, bilirubin-induced robust calcium flux in neurons, thus suggesting that an ionotropic, calcium-permeable receptor may underlie the bilirubin response. Transient receptor potential melastatin 2 (TRPM2), a member of the transient receptor potential superfamily of ion channels, was recently recognized as a bilirubin receptor.[17] To determine if blockade of TRPM2 was sufficient to reduce bilirubin-induced activity in NJG neurons, the selective TRPM2 inhibitor A23[17,18] was applied to neurons for 2 min prior to bilirubin exposure. A23 reduced bilirubin-induced calcium flux in NJG neurons (Figure 4K), thus supporting the role of TRPM2 as one of the bilirubin receptors expressed in these cells. Finally, to determine if bilirubin signaling and TRPM2 channel activity contribute to chronic SCD and SCF FMT-related pain, we assessed pain behaviors in SCD mice and SCD FMT recipients following A23 treatment. Oral administration of A23 reduced mechanical allodynia in SCD mice in a dose-dependent fashion (Figure 4L). A23 administration also decreased mechanical hypersensitivity in SCD FMT recipients (Figure 4M). Given the ubiquitous expression pattern of TRPM2,[19] A23 analgesia may result from inhibition of TRPM2 channels in vagal afferents or additional tissues. Regardless, TRPM2 is a novel target for persistent SCD pain relief.

BilR-expressing bacteria and TRPM2 are relevant targets for managing chronic SCD pain in humans

To assess whether the targets identified in the SCD mouse model translate to humans, heme catabolism dysregulation was first assessed in biospecimens collected from individuals with SCD (Figure 5A; Table S3). Heme catabolites were measured in the plasma of individuals with SCD since circulating metabolite signatures, particularly those generated by bacterial enzymes, are affected by gut dysbiosis.[20] Compared with age-matched healthy Black controls, individuals with SCD had significantly elevated levels of plasma biliverdin, bilirubin, and

Please cite this article in press as: Brandow et al., Gut microbiota and metabolites drive chronic sickle cell disease pain in mice, Cell Host & Microbe (2025), https://doi.org/10.1016/j.chom.2025.08.012

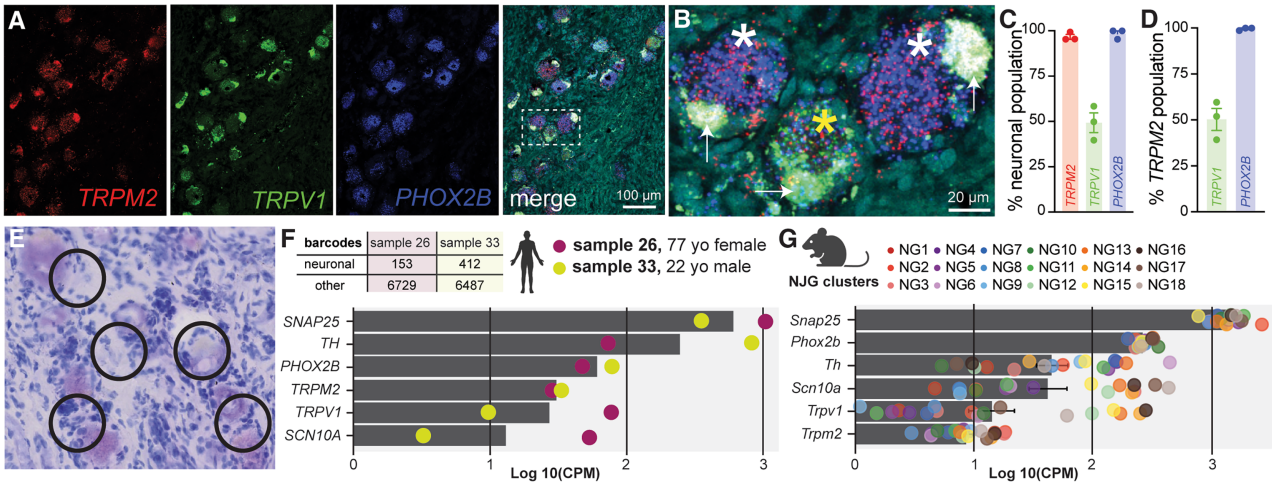

Figure 6. *TRPM2* is expressed in human nodose ganglia

(A) RNAscope *in situ* hybridization for *TRPM2* (red), *TRPV1* (green), *PHOX2B* (blue), and DAPI (cyan) in a human nodose ganglion.

(B) Magnified overlay image of outlined area in merged (A). White asterisks indicate *TRPM2*/*PHOX2B* positive neurons, the yellow asterisk labels a *TRPM2*/*PHOX2B*/*TRPV1* positive neuron, and white arrows point to background lipofuscin stain. *TRPM2* was also detected in a subset of non-neuronal cells.

(C) Percentage of total nodose ganglion neurons that were positive for *TRPM2* (97%), TRPV1 (49%), and *PHOX2B* (98%) across three donors.

(D) Percentage of *TRPM2*-positive nodose ganglion neurons that co-expressed TRPV1 (50%) or *PHOX2B* (100%).

(E) H&E stained section of human nodose ganglion highlighting neuronal barcodes.

(F) Results of spatial transcriptomic analysis performed on 565 neuronal barcodes sampled across the nodose ganglion from two tissue donors. Pseudobulk analysis of human nodose neuronal barcodes revealed expression of tissue-relevant genes, including *TRPM2*.

(G) Publicly available single-cell RNA sequencing dataset also reveals *Trpm2* is expressed in all previously described mouse nodose ganglia molecular clusters.[23]

urobilinogen during baseline state of health (defined as the absence of an acute disease exacerbation within 2 weeks of biospecimen collection; Figures 5B–5F). Heme catabolite levels were not further elevated when sampled from the same individual during an acute pain episode (paired data; Figures 5B–5F). These data confirmed that heme catabolism products, some of which are only degraded via microbial enzymes, are persistently elevated in individuals with SCD, and thus, may contribute to chronic SCD pain, while acute SCD pain episodes are driven by additional mechanisms.

Bilirubin reductase (BilR), a gene expressed by many Firmicutes found in human intestines, was recently identified as the enzyme responsible for metabolizing bilirubin to urobilinogen (Figure 5G).[13] Considering that individuals with SCD have chronically elevated levels of bilirubin in circulation and thus likely have similarly high levels of bilirubin in the gut throughout their lives, we hypothesized that the abundance of gut-resident BilR-expressing bacteria would differ between individuals with SCD and healthy controls. To assess this possibility, 16S rRNA gene sequencing was performed on stool samples collected from individuals with SCD and related and unrelated healthy Black controls (Figure 5H; Table S4). Of the 125 genera that are known BilR producers, 28 were identified in our dataset, and 8 were found to be differentially abundant in individuals with SCD relative to controls (Figure 5I). When the total abundance of BilR producers was summed for individual participants, individuals with SCD were found to have lower levels of BilR-producing bacteria in their stool as compared with healthy pain-free controls (Figure 5J). Notably, genera that express the long form of the *bilR* gene were decreased in abundance in SCD patient stool, whereas genera that express the short *bilR* sequence were increased in abundance in SCD patients (Figure 5K). Given that both the short and long *bilR* transcripts translate into proteins that effectively reduce bilirubin,[13] this gene length-based discrimination was a surprising finding that requires further study in the future.

In addition to measuring bilirubin catabolism in individuals with SCD, RNAscope *in situ* hybridization and transcriptomic analyses were completed on human nodose ganglia tissue to investigate the expression pattern of *TRPM2*, among other putative drug targets (Table S5). RNAscope revealed that 97% of human nodose neurons express *TRPM2* (Figures 6A–6C). Every single *TRPM2*-positive neuron also expressed *PHOX2B*, a transcription factor that selectively marks placode-derived cranial sensory ganglia.[21] Roughly 50% of *TPRM2*-positive neurons also expressed transient receptor potential vanilloid 1 (*TRPV1*), a putative nociceptor marker (Figure 6D). Comprehensive analysis of human nodose ganglia gene expression was next performed using the 10× Genomics Visium spatial gene expression platform. In this platform, tissue is mounted onto slides containing 55 μm barcoded spots wherein the mRNAs within each spot are spatially registered and sequenced (Figure 5E). Given the average size of human sensory ganglia neuronal soma (20–120 μm[22]), this technique allows for nearly single-neuron resolution of human nodose ganglia gene expression. A total of 565 neuronal barcodes were identified across tissue from two donors (Figure 6F). Pseudobulk analysis of human nodose ganglia neurons and previously published single-cell RNA sequencing data from mouse[23] revealed similar expression levels of general neuronal markers (*SNAP25*, encodes synaptosomal-associated protein 25 kDa), nodose ganglia-specific neuronal markers (*PHOX2B*), and putative nociceptor markers (*TRPV1*; *SCN10A*,

Please cite this article in press as: Brandow et al., Gut microbiota and metabolites drive chronic sickle cell disease pain in mice, Cell Host & Microbe (2025), https://doi.org/10.1016/j.chom.2025.08.012

encodes $Na_v1.8$) between species. Importantly, *TRPM2* expression was also detected in both human samples and across all 18 nodose ganglia neuronal clusters reported in mouse (Figures 6F and 6G). Given these data, TRPM2 is a translationally relevant target that should be the focus of future SCD pain therapeutics.

DISCUSSION

Herein, we identified specific gut bacteria and host metabolites that drive chronic SCD pain. Specifically, we determined that the contents of the SCD mouse gastrointestinal tract, when transplanted into an otherwise naive animal, induce widespread pain that closely mirrors pain behaviors exhibited by SCD fecal donors. This pain is driven by bilirubin signaling through TRPM2 channels.Bilirubin, a heme breakdown product that is catabolized by gut bacteria, directly activates and increases the excitability of vagal afferents, leading to central sensitization. In a reciprocal fashion, transplant of a healthy gut microbiota into SCD mice temporarily alleviates chronic pain in recipient animals. This analgesic effect results, in part, from increased abundance of *Akkermansia muciniphila* in the gastrointestinal milieu. Supplementation with *A. muciniphila* probiotic reversed chronic pain in SCD mice but not through canonical mechanisms.

The identification of gastrointestinal bilirubin as a primary driver of chronic SCD pain is a novel discovery that is associated with many therapeutic opportunities. First, we demonstrated that inhibition of TRPM2 blocks bilirubin-induced calcium flux in a subset of nodose ganglia neurons and completely alleviates mechanical allodynia in SCD mice and mice that received SCD FMT. After performing the first known transcriptomic analysis of human nodose ganglia tissue, we confirmed that *TRPM2* mRNA is detected in human nodose ganglia neurons, thus confirming that targets identified in the SCD mouse model are translationally relevant. Excitement for this target is further compounded by additional TRPM2 endogenous agonists and expression patterns. TRPM2 channel activity and expression are directly modulated by lipopolysaccharide, tumor necrosis factor α, and reactive oxygen species,[19] all of which are elevated in both SCD mouse models and individuals with SCD.[24] TRPM2 is also present in many immune cells, endothelial cells, and microglia, all of which are implicated in SCD pathophysiology.[24] Thus, TRPM2 inhibitors may have additional on-target efficacy in managing SCD symptoms beyond chronic pain. It is likely that additional bilirubin receptors also contribute to SCD FMT-associated pain. The ionotropic serotonin receptor $5\text{-}HT_{3A}$[25] and G-protein-coupled receptor MRGPRX4 and its mouse homolog MRGPRA1[26] are other bilirubin receptors that should be explored as SCD analgesic targets.

In addition to preventing bilirubin-induced activity in extrinsic sensory neurons, chemical or probiotic therapies that reduce gastrointestinal bilirubin should be further studied to determine their efficacy in SCD pain management. Reduced circulating bilirubin is a hallmark of success for SCD-modifying therapies that decrease hemolysis, and HU is one such drug that works in this manner. Notably, few, limited sample size studies have explored the relationship between long-term HU use and chronic SCD pain. In one study, HU decreased self-reported daily pain intensity,[27] and in a second study, individuals with SCD taking HU had higher heat and mechanical pain thresholds compared with individuals not actively taking the drug[28] (i.e., individuals taking HU were less sensitive to heat and mechanical pain). Probiotic bacteria that express BilR should also be studied to determine their efficacy in SCD pain and symptom management. Of the BilR-expressing bacteria that were decreased in SCD patient stool, *Holdemanella* is a particularly exciting probiotic candidate. In addition to expressing BilR, *Holdemanella biformis* and its mouse homolog *Faecalibaculum rodentium* produce SCFAs,[29] anti-inflammatory compounds that are decreased in the SCD mouse gut. Notably, many *Holdemanella* species are beta-lactam susceptible.[30] Children with SCD are prescribed daily prophylactic beta-lactam treatment for the first 6 years of life to prevent pneumococcal sepsis.[31] Although we do not have accurate beta-lactam prescription and adherence information for participants enrolled in this study, the decreased *Holdemanella* abundance may be a long-lasting change resulting from this standard-of-care treatment. Thus, therapeutically increasing *Holdmanella* abundance may be an especially effective treatment option for individuals with SCD who adhered to early-life penicillin regimens. Finally, our studies also identified *Akkermansia* as an important non-BilR-expressing bacteria that is also decreased in the SCD gut. Future studies will examine novel mechanisms through which *Akkermansia* treatment decreases SCD pain given that the previously described mechanisms do not seem to account for the analgesia observed in these experiments.

Limitations of the study

Due to sample collection limitations, bilirubin measurements in SCD patient and healthy control stool are notably omitted from this study. Intestinal bilirubin is rapidly metabolized into urobilinogen; thus, it is unclear if levels of colonic bilirubin are ever sufficiently high enough to engage TRPM2 receptors expressed on extrinsic sensory afferents. However, given the decreased abundance of BilR-expressing bacteria and systemically elevated levels of plasma bilirubin in SCD patients, it is possible that SCD is a unique chronic pain condition characterized by persistent, supra-physiological levels of bilirubin both in and out of the gut. Future studies should assess potential correlations between both stool and serum bilirubin levels and chronic pain measures in individuals with SCD. Related to this, we would be remiss to not reemphasize the body-wide expression patterns of TRPM2. Since bilirubin levels are chronically elevated in blood, the analgesia observed in SCD mice following systemic administration of TRPM2 inhibitors may very well result from inhibition of bilirubin-TRPM2 signaling outside of the intestine. Finally, our *in vitro* data clearly highlight that additional, non-TRPM2 bilirubin receptors are expressed in nodose ganglia neurons and thus likely contribute to SCD FMT and chronic SCD pain. Knowing this, future studies should assess the relative contributions of all bilirubin receptors expressed in extrinsic sensory afferents, and subsequent therapeutic development should be prioritized based on these results.

In closing, we have identified several novel non-opioid-based targets for the management of chronic SCD pain. Given the long-term negative consequences of opioid use, the race-based obstacles that many individuals with SCD face when trying to access opioids,[32] and the often-inadequate analgesia that results from taking opioid drugs, non-opioid therapies are desperately

needed for individuals with SCD. Our detailed characterization of host-microbe interactions in SCD significantly advances the understanding of chronic SCD pain pathophysiology and provides the framework for microbial therapeutics in this patient population.

RESOURCE AVAILABILITY

Lead contact

All correspondence should be addressed to the lead contact, Katelyn Sadler (katelyn.sadler@utdallas.edu).

Materials availability

This study did not generate novel reagents, bacterial strains, or mice.

Data and code availability

- All nodose ganglia sequencing data are deposited in dbGaP: phs001158.v4.p2 and SPARC (https://doi.org/10.26275/6vkg-lpxp).
- This paper does not report any original code.
- All additional data are available in the main text or the supplementary materials.

ACKNOWLEDGMENTS

The authors would like to thank the following: individuals with SCD and those without SCD who donated biospecimens; organ donors whose tissue was used in these studies; family members of both biospecimen and tissue donors; clinical research coordinators in the Brandow Lab who enrolled and collected biospecimens; Southwest Transplant Alliance for supporting human tissue recovery efforts; Dr. Liangren Zhang and lab for the generous gift of A23 compound; Dr. Ashley Plumb, Nya Gayluak, and Raina Karakkattil for assistance with tissue collection; Dr. Xintong Dong for *S. aureus* cultures; Dr. Lena Nguyen and lab for use of the real-time quantitative PCR machine; members of the Sadler Lab, Stucky Lab—in particular, Tony Menzel—and the Center for Advanced Pain Studies for their constant curiosity and constructive feedback on this project. This work was funded by National Institutes of Health grants to K.E.S. (K99HL155791 and R00HL155791), A.M.B. (R01HL142657, R61NS114954, R33NS114954, and K23HL114636), T.J.P. (U19NS130608), N.H.S. (R35GM122503), and C.L.S. (R01NS070711 and R37NS108278). Additional support was provided by the Rita Allen Foundation (Award in Pain to K.E.S.) and the Advancing a Healthier Wisconsin Endowment Research and Education Initiative Fund (C.L.S.).

AUTHOR CONTRIBUTIONS

Conceptualization, K.E.S. and A.M.B.; methodology, K.E.S., S.N.A., Z.M., V.L.E., I.M., S.M., A.K., S.I.S., K.M., S.A., A.S., M.K.S., T.B.W., and M.H.; investigation, K.E.S., S.N.A., Z.M., V.L.E., M.L.P., I.M., S.M., A.K., S.I.S., K.M., M.A.S., J.C.R., D.T.-F., I.S., M.K.S., T.B.W., M.H., D.M.R.G., and A.M.B.; visualization, K.E.S., S.N.A., Z.M., K.M., and S.I.S.; funding acquisition, K.E.S., A.M.B., N.H.S., K.L.P., C.L.S., and T.J.P.; supervision, K.E.S., A.M.B., I.M., G.D., N.H.S., K.L.P., C.L.S., and T.J.P.; writing – original draft, K.E.S.; and writing – review and editing, K.E.S., A.M.B., S.N.A., Z.M., V.L.E., M.L.P., I.M., S.M., A.K., S.I.S., K.M., M.A.S., S.A., A.S., J.C.R., D.T.-F., I.S., M.K.S., T.B.W., M.H., D.M.R.G., G.D., N.H.S., C.L.S., and T.J.P.

DECLARATION OF INTERESTS

The authors declare no competing interests.

STAR★METHODS

Detailed methods are provided in the online version of this paper and include the following:

- KEY RESOURCES TABLE
- EXPERIMENTAL MODELS AND STUDY PARTICIPANT DETAILS
  - Mouse strains
  - Akkermansia muciniphila
- PLASMA AND STOOL SAMPLE DONORS
  - Plasma analysis
  - Stool analysis
  - Nodose ganglia tissue donors
- METHOD DETAILS
  - Animal treatments
  - Behavior tests
  - Sample preparation for 16S ribosomal RNA gene sequencing
  - 16S ribosomal RNA gene sequencing
  - Immunofluorescent staining
  - Gut permeability
  - Bacterial translocation assessment
  - Probiotic DNA extraction, amplification, and species confirmation
  - Quantitative real-time PCR of gap junction genes
  - Nodose/jugular ganglia calcium imaging and electrophysiology
  - Metabolite screens
  - RNAscope *in situ* hybridization
  - Human nodose ganglia spatial transcriptomics
- QUANTIFICATION AND STATISTICAL ANALYSIS

SUPPLEMENTAL INFORMATION

Supplemental information can be found online at https://doi.org/10.1016/j.chom.2025.08.012.

Received: March 10, 2025
Revised: July 23, 2025
Accepted: August 25, 2025

REFERENCES

1. Badawy, S.M., Beg, U., Liem, R.I., Chaudhury, S., and Thompson, A.A. (2021). A systematic review of quality of life in sickle cell disease and thalassemia after stem cell transplant or gene therapy. Blood Adv. *5*, 570–583. https://doi.org/10.1182/BLOODADVANCES.2020002948.
2. Brim, H., Taylor, J., Abbas, M., Vilmenay, K., Daremipouran, M., Varma, S., Lee, E., Pace, B., Song-Naba, W.L., Gupta, K., et al. (2021). The gut microbiome in sickle cell disease: Characterization and potential implications. PLoS One *16*, e0255956. https://doi.org/10.1371/journal.pone.0255956.
3. Lim, S.H., Morris, A., Li, K., Fitch, A.C., Fast, L., Goldberg, L., Quesenberry, M., Sprinz, P., and Methé, B. (2018). Intestinal Microbiome Analysis Revealed Dysbiosis in Sickle Cell Disease. Am. J. Hematol. *93*, E91–E93.
4. Wu, L.C., Sun, C.W., Ryan, T.M., Pawlik, K.M., Ren, J., and Townes, T.M. (2006). Correction of sickle cell disease by homologous recombination in embryonic stem cells. Blood *108*, 1183–1188. https://doi.org/10.1182/blood-2006-02-004812.
5. Luo, Y., Lan, C., Li, H., Ouyang, Q., Kong, F., Wu, A., Ren, Z., Tian, G., Cai, J., Yu, B., et al. (2022). Rational consideration of Akkermansia muciniphila targeting intestinal health: advantages and challenges. npj Biofilms Microbiomes *8*, 81. https://doi.org/10.1038/s41522-022-00338-4.
6. Li, Z., Hu, G., Zhu, L., Sun, Z., Jiang, Y., Gao, M.J., and Zhan, X. (2021). Study of growth, metabolism, and morphology of Akkermansia muciniphila with an in vitro advanced bionic intestinal reactor. X. BMC Microbiol. *21*, 61. https://doi.org/10.1186/S12866-021-02111-7.
7. Dutta, D., Methe, B., Amar, S., Morris, A., and Lim, S.H. (2019). Intestinal injury and gut permeability in sickle cell disease. J. Transl. Med. *17*, 1–4. https://doi.org/10.1186/S12967-019-1938-8/FIGURES/2.
8. Poplawska, M., Dutta, D., Jayaram, M., Chong, N.S., Salifu, M., and Lim, S.H. (2022). Genes modulating intestinal permeability and microbial community are dysregulated in sickle cell disease. Ann. Hematol. *101*, 1009–1013. https://doi.org/10.1007/s00277-022-04794-y.

9. Poplawska, M., Dutta, D., Jayaram, M., Salifu, M., Chong, N.S., and Lim, S.H. (2022). Intestinal pathophysiological abnormalities in steady state and after vaso-occlusive crisis in murine sickle cell disease. Br. J. Haematol. *196*, 777–780. https://doi.org/10.1111/BJH.17889.

10. Lewis, C.V., Sellak, H., Sawan, M.A., Joseph, G., Darby, T.M., VanInsberghe, D., Naudin, C.R., Archer, D.R., Jones, R.M., and Taylor, W.R. (2023). Intestinal barrier dysfunction in murine sickle cell disease is associated with small intestine neutrophilic inflammation, oxidative stress, and dysbiosis. FASEB Bioadv. *5*, 199–210. https://doi.org/10.1096/FBA.2022-00121.

11. Brandow, A.M., Stucky, C.L., Hillery, C.A., Hoffmann, R.G., and Panepinto, J.A. (2013). Patients with sickle cell disease have increased sensitivity to cold and heat. Am. J. Hematol. *88*, 37–43. https://doi.org/10.1002/ajh.23341.

12. Sadler, K.E., Zappia, K.J., O'Hara, C.L., Langer, S.N., Weyer, A.D., Hillery, C.A., and Stucky, C.L. (2018). Chemokine (c-c motif) receptor 2 mediates mechanical and cold hypersensitivity in sickle cell disease mice. Pain *159*, 1652–1663. https://doi.org/10.1097/j.pain.0000000000001253.

13. Hall, B., Levy, S., Dufault-Thompson, K., Arp, G., Zhong, A., Ndjite, G.M., Weiss, A., Braccia, D., Jenkins, C., Grant, M.R., et al. (2024). BilR is a gut microbial enzyme that reduces bilirubin to urobilinogen. Nat. Microbiol. *9*, 173–184. https://doi.org/10.1038/s41564-023-01549-x.

14. Charache, S., Terrin, M.L., Moore, R.D., Dover, G.J., Barton, F.B., Eckert, S.V., McMahon, R.P., and Bonds, D.R. (1995). Effect of Hydroxyurea on the Frequency of Painful Crises in Sickle Cell Anemia. Investigators of the Multicenter Study of Hydroxyurea in Sickle Cell Anemia. N. Engl. J. Med. *332*, 1317–1322. https://doi.org/10.1056/NEJM199505183322001.

15. Voskaridou, E., Christoulas, D., Bilalis, A., Plata, E., Varvagiannis, K., Stamatopoulos, G., Sinopoulou, K., Balassopoulou, A., Loukopoulos, D., and Terpos, E. (2010). The effect of prolonged administration of hydroxyurea on morbidity and mortality in adult patients with sickle cell syndromes: results of a 17-year, single-center trial (LaSHS). Blood *115*, 2354–2363. https://doi.org/10.1182/BLOOD-2009-05-221333.

16. Gao, Y.-J., and Ji, R.-R. (2009). c-Fos and pERK, which is a better marker for neuronal activation and central sensitization after noxious stimulation and tissue injury? Open Pain J. *2*, 11–17. https://doi.org/10.2174/1876386300902010011.

17. Liu, H.W., Gong, L.N., Lai, K., Yu, X.F., Liu, Z.Q., Li, M.X., Yin, X.L., Liang, M., Shi, H.S., Jiang, L.H., et al. (2023). Bilirubin gates the TRPM2 channel as a direct agonist to exacerbate ischemic brain damage. Neuron *111*, 1609–1625.e6. https://doi.org/10.1016/J.NEURON.2023.02.022.

18. Zhang, H., Yu, P., Lin, H., Jin, Z., Zhao, S., Zhang, Y., Xu, Q., Jin, H., Liu, Z., Yang, W., et al. (2021). The Discovery of Novel ACA Derivatives as Specific TRPM2 Inhibitors that Reduce Ischemic Injury Both In Vitro and In Vivo. J. Med. Chem. *64*, 3976–3996. https://doi.org/10.1021/ACS.JMEDCHEM.0C02129.

19. Sumoza-Toledo, A., and Penner, R. (2011). TRPM2: a multifunctional ion channel for calcium signalling. J. Physiol. *589*, 1515–1525. https://doi.org/10.1113/JPHYSIOL.2010.201855.

20. Dekkers, K.F., Sayols-Baixeras, S., Baldanzi, G., Nowak, C., Hammar, U., Nguyen, D., Varotsis, G., Brunkwall, L., Nielsen, N., Eklund, A.C., et al. (2022). An online atlas of human plasma metabolite signatures of gut microbiome composition. Nat. Commun. *13*, 5370. https://doi.org/10.1038/s41467-022-33050-0.

21. Dauger, S., Pattyn, A., Lofaso, F., Gaultier, C., Goridis, C., Gallego, J., and Brunet, J.F. (2003). Phox2b controls the development of peripheral chemoreceptors and afferent visceral pathways. Development *130*, 6635–6642. https://doi.org/10.1242/DEV.00866.

22. Nagashima, K., and Oota, K. (1974). A HISTOPATHOLOGICAL STUDY OF THE HUMAN SPINAL GANGLIA. NORMAL VARIATIONS IN AGING. Acta Pathol. Jpn. *24*, 333–344. https://doi.org/10.1111/J.1440-1827.1974.TB00827.X.

23. Kupari, J., Häring, M., Agirre, E., Castelo-Branco, G., and Ernfors, P. (2019). An Atlas of Vagal Sensory Neurons and Their Molecular Specialization. Cell Rep. *27*, 2508–2523.e4. https://doi.org/10.1016/j.celrep.2019.04.096.

24. Tran, H., Gupta, M., and Gupta, K. (2017). Targeting novel mechanisms of pain in sickle cell disease. Blood *130*, 2377–2385. https://doi.org/10.1182/BLOOD-2017-05-782003.

25. Kong, E., Wang, H., Wang, X., Zhang, Y., Zhang, J., Yu, W., Feng, X., Sun, Y., and Wu, F. (2021). Bilirubin Induces Pain Desensitization in Cholestasis by Activating 5-Hydroxytryptamine 3A Receptor in Spinal Cord. Front. Cell Dev. Biol. *9*, 605855.

26. Meixiong, J., Vasavda, C., Green, D., Zheng, Q., Qi, L., Kwatra, S.G., Hamilton, J.P., Snyder, S.H., and Dong, X. (2019). Identification of a bilirubin receptor that may mediate a component of cholestatic itch. eLife *8*, e44116. https://doi.org/10.7554/eLife.44116.

27. Smith, W.R., Ballas, S.K., Mccarthy, W.F., Bauserman, R.L., Swerdlow, P.S., Steinberg, M.H., and Waclawiw, M.A. (2011). The Association Between Hydroxyurea Treatment and Pain Intensity, Analgesic Use, and Utilization in Ambulatory Sickle Cell Anemia Patients. Pain Med. *12*, 697–705. https://doi.org/10.1111/J.1526-4637.2011.01096.X/2/PME_1096_F2.JPEG.

28. Letzen, J.E., Lanzkron, S., Bond, K., Carroll, C.P., Haythornthwaite, J.A., Nance, S., and Campbell, C.M. (2019). Preliminary evidence that hydroxyurea is associated with attenuated peripheral sensitization in adults with sickle cell disease. PAIN Rep. *4*, e724. https://doi.org/10.1097/PR9.0000000000000724.

29. Zagato, E., Pozzi, C., Bertocchi, A., Schioppa, T., Saccheri, F., Guglietta, S., Fosso, B., Melocchi, L., Nizzoli, G., Troisi, J., et al. (2020). Endogenous murine microbiota member Faecalibaculum rodentium and its human homologue protect from intestinal tumour growth. Nat. Microbiol. *5*, 511–524. https://doi.org/10.1038/s41564-019-0649-5.

30. Schwartz, D.J., Langdon, A., Sun, X., Langendorf, C., Berthé, F., Grais, R.F., Trehan, I., Isanaka, S., and Dantas, G. (2023). Effect of amoxicillin on the gut microbiome of children with severe acute malnutrition in Madarounfa, Niger: a retrospective metagenomic analysis of a placebo-controlled trial. Lancet Microbe *4*, e931–e942. https://doi.org/10.1016/S2666-5247(23)00213-6.

31. Gaston, M.H., Verter, J.I., Woods, G., Pegelow, C., Kelleher, J., Presbury, G., Zarkowsky, H., Vichinsky, E., Iyer, R., and Lobel, J.S. (1986). Prophylaxis with Oral Penicillin in Children with Sickle Cell Anemia. A randomized trial. N. Engl. J. Med. *314*, 1593–1599. https://doi.org/10.1056/NEJM198606193142501.

32. Power-Hays, A., and McGann, P.T. (2020). When Actions Speak Louder Than Words — Racism and Sickle Cell Disease. N. Engl. J. Med. *383*, 1902–1903. https://doi.org/10.1056/NEJMp2022125.

33. Mao, D.P., Zhou, Q., Chen, C.Y., and Quan, Z.X. (2012). Coverage evaluation of universal bacterial primers using the metagenomic datasets. BMC Microbiol. *12*, 66. https://doi.org/10.1186/1471-2180-12-66.

34. Muyzer, G., De Waal, E.C., and Uitterlinden, A.G. (1993). Profiling of complex microbial populations by denaturing gradient gel electrophoresis analysis of polymerase chain reaction-amplified genes coding for 16S rRNA. Appl. Environ. Microbiol. *59*, 695–700. https://doi.org/10.1128/AEM.59.3.695-700.1993.

35. Earley, H., Lennon, G., Balfe, Á., Coffey, J.C., Winter, D.C., and O'Connell, P.R. (2019). The abundance of Akkermansia muciniphila and its relationship with sulphated colonic mucins in health and ulcerative colitis. Sci. Rep. *9*, 15683. https://doi.org/10.1038/S41598-019-51878-3.

36. Bolyen, E., Rideout, J.R., Dillon, M.R., Bokulich, N.A., Abnet, C.C., Al-Ghalith, G.A., Alexander, H., Alm, E.J., Arumugam, M., Asnicar, F., et al. (2019). Reproducible, interactive, scalable and extensible microbiome data science using QIIME 2. Nat. Biotechnol. *37*, 852–857. https://doi.org/10.1038/s41587-019-0209-9.

37. Derrien, M., Vaughan, E.E., Plugge, C.M., and de Vos, W.M. (2004). Akkermansia municiphila gen. nov. Int. J. Syst. Evol. Microbiol. *54*, 1469–1476. https://doi.org/10.1099/IJS.0.02873-0.

38. Miller, R.S., and Hoskins, L.C. (1981). Mucin degradation in human colon ecosystems: Fecal population densities of mucin-degrading bacteria

estimated by a "most probable number" method. Gastroenterology *81*, 759–765. https://doi.org/10.1016/0016-5085(81)90503-5.

39. Dixon, W.J. (1965). The Up-and-Down Method for Small Samples. J. Am. Stat. Assoc. *60*, 967–978. https://doi.org/10.1080/01621459.1965.10480843.
40. Chaplan, S.R., Bach, F.W., Pogrel, J.W., Chung, J.M., and Yaksh, T.L. (1994). Quantitative assessment of tactile allodynia in the rat paw. J. Neurosci. Methods *53*, 55–63. https://doi.org/10.1016/0165-0270(94)90144-9.
41. Brenner, D.S., Golden, J.P., and Gereau, R.W. (2012). A novel behavioral assay for measuring cold sensation in mice. PLoS One *7*, e39765. https://doi.org/10.1371/journal.pone.0039765.
42. Hargreaves, K., Dubner, R., Brown, F., Flores, C., and Joris, J. (1988). A new and sensitive method for measuring thermal nociception in cutaneous hyperalgesia. Pain *32*, 77–88. https://doi.org/10.1016/0304-3959(88)90026-7.
43. Kommineni, S., Bretl, D.J., Lam, V., Chakraborty, R., Hayward, M., Simpson, P., Cao, Y., Bousounis, P., Kristich, C.J., and Salzman, N.H. (2015). Bacteriocin production augments niche competition by enterococci in the mammalian gastrointestinal tract. Nature *526*, 719–722. https://doi.org/10.1038/NATURE15524.
44. Caporaso, J.G., Lauber, C.L., Walters, W.A., Berg-Lyons, D., Huntley, J., Fierer, N., Owens, S.M., Betley, J., Fraser, L., Bauer, M., et al. (2012). Ultra-high-throughput microbial community analysis on the Illumina HiSeq and MiSeq platforms. ISME J. *6*, 1621–1624. https://doi.org/10.1038/ismej.2012.8.
45. Martin, M. (2011). Cutadapt removes adapter sequences from high-throughput sequencing reads. EMBnet J. *17*, 10–12. https://doi.org/10.14806/EJ.17.1.200.
46. Callahan, B.J., McMurdie, P.J., Rosen, M.J., Han, A.W., Johnson, A.J.A., and Holmes, S.P. (2016). DADA2: High-resolution sample inference from Illumina amplicon data. Nat. Methods *13*, 581–583. https://doi.org/10.1038/nmeth.3869.
47. Katoh, K., and Standley, D.M. (2013). MAFFT Multiple Sequence Alignment software version 7: Improvements in performance and usability. Mol. Biol. Evol. *30*, 772–780. https://doi.org/10.1093/MOLBEV/MST010.
48. Lane, D. (1991). 16S/23S rRNA sequencing. In Nucleic Acid Technique in Bacterial Systematics (Wiley).
49. Price, M.N., Dehal, P.S., and Arkin, A.P. (2010). FastTree 2 - Approximately maximum-likelihood trees for large alignments. PLoS One *5*, e9490. https://doi.org/10.1371/journal.pone.0009490.
50. Yilmaz, P., Parfrey, L.W., Yarza, P., Gerken, J., Pruesse, E., Quast, C., Schweer, T., Peplies, J., Ludwig, W., and Glöckner, F.O. (2014). The SILVA and "all-species Living Tree Project (LTP)" taxonomic frameworks. Nucleic Acids Res. *42*, D643–D648. https://doi.org/10.1093/nar/gkt1209.
51. Quast, C., Pruesse, E., Yilmaz, P., Gerken, J., Schweer, T., Yarza, P., Peplies, J., and Glöckner, F.O. (2013). The SILVA ribosomal RNA gene database project: Improved data processing and web-based tools. Nucleic Acids Res. *41*, D590–D596. https://doi.org/10.1093/nar/gks1219.
52. Anderson, M.J. (2001). A new method for non-parametric multivariate analysis of variance. Austral Ecol. *26*, 32–46. https://doi.org/10.1046/j.1442-9993.2001.01070.x.
53. Caporaso, J.G., Kuczynski, J., Stombaugh, J., Bittinger, K., Bushman, F.D., Costello, E.K., Fierer, N., Pẽa, A.G., Goodrich, J.K., Gordon, J.I., et al. (2010). QIIME Allows Analysis of High-Throughput Community Sequencing Data. Nat. Methods *7*, 335–336. https://doi.org/10.1038/nmeth.f.303.
54. Kruskal, W.H., and Wallis, W.A. (1952). Use of Ranks in One-Criterion Variance Analysis. J. Am. Stat. Assoc. *47*, 583–621. https://doi.org/10.1080/01621459.1952.10483441.
55. Vázquez-Baeza, Y., Pirrung, M., Gonzalez, A., and Knight, R. (2013). EMPeror: A tool for visualizing high-throughput microbial community data. GigaScience *2*, 16. https://doi.org/10.1186/2047-217X-2-16.
56. Vázquez-Baeza, Y., Gonzalez, A., Smarr, L., McDonald, D., Morton, J.T., Navas-Molina, J.A., and Knight, R. (2017). Bringing the Dynamic Microbiome to Life with Animations. Cell Host Microbe *21*, 7–10. https://doi.org/10.1016/j.chom.2016.12.009.
57. Bisanz, J. (2018). qiime2R: Importing QIIME2 artifacts and associated data into R sessions. GitHub. http://github.com/jbisanz/qiime2R.
58. RStudio Team (2022). RStudio: Integrated Development for R. PBC. http://www.rstudio.com/.
59. R Core Team (2022). R: A Language and Environment for Statistical Computing. R Foundation for Statistical Computing, Vienna. https://www.R-project.org.
60. Segata, N., Izard, J., Waldron, L., Gevers, D., Miropolsky, L., Garrett, W.S., and Huttenhower, C. (2011). Metagenomic biomarker discovery and explanation. Genome Biol. *12*, R60. https://doi.org/10.1186/gb-2011-12-6-r60.
61. Mallick, H., Rahnavard, A., McIver, L.J., Ma, S., Zhang, Y., Nguyen, L.H., Tickle, T.L., Weingart, G., Ren, B., Schwager, E.H., et al. (2021). Multivariable association discovery in population-scale meta-omics studies. PLoS Comput. Biol. *17*, e1009442. https://doi.org/10.1371/JOURNAL.PCBI.1009442.
62. Monasterio, G., Morales, R.A., Bejarano, D.A., Abalo, X.M., Fransson, J., Larsson, L., Schlitzer, A., Lundeberg, J., Das, S., and Villablanca, E.J. (2024). A versatile tissue-rolling technique for spatial-omics analyses of the entire murine gastrointestinal tract. Nat. Protoc. *19*, 3085–3137. https://doi.org/10.1038/s41596-024-01001-2.
63. Melhem, H., Kaya, B., Kaymak, T., Wuggenig, P., Flint, E., Roux, J., Oost, K.C., Cavelti-Weder, C., Balmer, M.L., Walser, J.C., et al. (2022). Epithelial GPR35 protects from Citrobacter rodentium infection by preserving goblet cells and mucosal barrier integrity. Mucosal Immunol. *15*, 443–458. https://doi.org/10.1038/S41385-022-00494-Y;KWRD=BIOMEDICINE.
64. Babic, T., Townsend, R.L., Patterson, L.M., Sutton, G.M., Zheng, H., and Berthoud, H.R. (2009). Phenotype of neurons in the nucleus of the solitary tract that express CCK-induced activation of the ERK signaling pathway. Am. J. Physiol. Regul. Integr. Comp. Physiol. *296*, R845–R854. https://doi.org/10.1152/AJPREGU.90531.2008.
65. Shiers, S., Sahn, J.J., and Price, T.J. (2023). MNK1 and MNK2 Expression in the Human Dorsal Root and Trigeminal Ganglion. Neuroscience *515*, 96–107. https://doi.org/10.1016/J.NEUROSCIENCE.2023.01.039.
66. Tavares-Ferreira, D., Shiers, S., Ray, P.R., Wangzhou, A., Jeevakumar, V., Sankaranarayanan, I., Cervantes, A.M., Reese, J.C., Chamessian, A., Copits, B.A., et al. (2022). Spatial transcriptomics of dorsal root ganglia identifies molecular signatures of human nociceptors. Sci. Transl. Med. *14*, eabj8186. https://doi.org/10.1126/SCITRANSLMED.ABJ8186.

Please cite this article in press as: Brandow et al., Gut microbiota and metabolites drive chronic sickle cell disease pain in mice, Cell Host & Microbe (2025), https://doi.org/10.1016/j.chom.2025.08.012

CellPress

STAR★METHODS

KEY RESOURCES TABLE

REAGENT or RESOURCE	SOURCE	IDENTIFIER
Antibodies		
Rabbit polyclonal anti-MUC2	Abcam	#AB90007; RRID: AB_10713220
Rabbit polyclonal anti-pERK1/2	Cell Signaling Technology	#9101; RRID: AB_2315036
Mouse monoclonal anti-NeuN	Sigma-Aldrich	#MAB; RRID: AB_2940866
Bacterial strains		
Akkermansia muciniphila	Pendulum	N/A
Biological samples		
Human nodose ganglia	Southwest Transplant Alliance Anabios	https://www.organ.org/ https://anabios.com/
Chemicals		
Ampicillin	Sigma-Aldrich	#A9393
FITC-dextran	Sigma-Aldrich	#FD4
Hydroxyurea	Sigma-Aldrich	#H8627
Bilirubin	Millipore	#2011
A23, TRPM2 inhibitor	Gift from Dr. Liangren Zhang	N/A
SSC buffer 20X concentrate	Sigma-Aldrich	#S6639
Critical commercial assays		
DNeasy Powerlyzer Powersoil Kit	Qiagen	#12855-100
Bilirubin assay kit	Sigma-Aldrich	MAK126
RNeasy Plus Universal Mini Kit	Qiagen	#73404
QuantiTect Reverse Transcription Kit	Qiagen	#205311
PowerUp™ SYBR™ Green Master Mix	Applied Biosystems	#A25742
RNAscope Multiplex Fluorescent V2 Assay	Advanced Cell Diagnostics	#323100
Protease III reagent	Advanced Cell Diagnostics	#322381
RNAscope wash buffer	Advanced Cell Diagnostics	#310091
TSA buffer	Advanced Cell Diagnostics	#322809
HRP blocker	Advanced Cell Diagnostics	#323110
TSA Plus fluorescein detection kit	Ayoka Biosciences	#NEL741001KT
TSA Plus cyanine 3 (Cy3) detection kit	Ayoka Biosciences	#NEL744001KT
TSA Plus cyanine5 (Cy5) detection kit	Ayoka Biosciences	#NEL745001KT
RNAscope 3-plex positive control probe	Advanced Cell Diagnostics	#320861
RNAscope 3-plex negative control probe	Advanced Cell Diagnostics	#320871
Visium Spatial Tissue Optimization Slide & Reagent	10X Genomics	PN-1000193
Visium Spatial Gene Expression Slide & Reagent Kit	10X Genomics	PN-1000184
Experimental models: organisms/strains		
Mouse: C57BL/6J	The Jackson Laboratory	Strain #000664
Mouse: B6;129-*Hbb*$^{tm2(HBG1,HBB*)Tow}$/*Hbb*$^{tm3(HBG1,HBB)Tow}$ *Hba*$^{tm1(HBA)Tow}$/*J*	The Jackson Laboratory	Strain #013071
Oligonucleotides		
Muc2 forward primer: GATGGCACCTACCTCGTTGT	Integrated DNA Technologies	Poplawska et al.[8]
Muc2 reverse primer: GTCCTGGCACTTGTTGGAAT	Integrated DNA Technologies	Poplawska et al.[8]
Ocln forward primer: ACTCCTCCAATGGACAAGTG	Integrated DNA Technologies	Poplawska et al.[8]
Ocln reverse primer: CCCCACCTGTCGTGTAGTCT	Integrated DNA Technologies	Poplawska et al.[8]
Cldn2 forward primer: GTCATCGCCCATCAGAAGAT	Integrated DNA Technologies	Poplawska et al.[8]
Cldn2 reverse primer: ACTGTTGGACAGGGAACCAG	Integrated DNA Technologies	Poplawska et al.[8]

(*Continued on next page*)

Please cite this article in press as: Brandow et al., Gut microbiota and metabolites drive chronic sickle cell disease pain in mice, Cell Host & Microbe (2025), https://doi.org/10.1016/j.chom.2025.08.012

Continued

REAGENT or RESOURCE	SOURCE	IDENTIFIER
18S forward primer: GTAACCCGTTGAACCCCATT	Integrated DNA Technologies	Poplawska et al.[8]
18S reverse primer: CCATCCAATCGGTAGTAGCG	Integrated DNA Technologies	Poplawska et al.[8]
Universal bacteria forward primer: ACTCCTACGGGAGGCAGCAG	Integrated DNA Technologies	Mao et al.[33]
Universal bacteria reverse primer: 5′ATTACCGCGGCTGCTGG 3′	Integrated DNA Technologies	Muyzer et al.[34]
Akkermansia forward primer: CAGCACGTGAAGGTGGGGAC	Integrated DNA Technologies	Earley et al.[35]
Akkermansia reverse primer: CCTTGCGGTTGGCTTCAGAT	Integrated DNA Technologies	Earley et al.[35]
TRPM2 RNAscope probe	Advanced Cell Diagnostics	#577971-C1
TRPV1 RNAscope probe	Advanced Cell Diagnostics	#415381-C3
PHOX2B RNAscope probe	Advanced Cell Diagnostics	#567701-C2
Software and algorithms		
ImageJ	National Institutes of Health	https://imagej.net/ij/
QIIME2	https://qiime2.org	Bolyen et al.[36]
10X SpaceRanger	https://www.10xgenomics.com/support/software/space-ranger/downloads	version 1.1.0
10X Loupe Browser	https://www.10xgenomics.com/support/software/loupe-browser/downloads	version 5.0.1
R	R: The R Project for Statistical Computing	version 4.3.3
Seurat	https://satijalab.org/seurat/	version 5.1.0
ggplot2	https://cran.r-project.org/web/packages/ggplot2/index.html	version 3.5.1

EXPERIMENTAL MODELS AND STUDY PARTICIPANT DETAILS

Mouse strains

All animal protocols were in accordance with National Institute of Health guidelines and were approved by the Institutional Animal Care and Use Committees at the Medical College of Wisconsin (Milwaukee, WI; protocol #0383) and The University of Texas at Dallas (Richardson, TX; protocol #2022-0088). Animals were randomly assigned to treatment groups. The following mouse strains were used throughout the paper:

Townes transgenic mouse model of sickle cell disease (SCD).[4] In this knock-in model, mouse α-globin genes are replaced with human α-globin genes, and the major and minor mouse β-globin genes are replaced with either: (1) normal human γ and human β-globin genes (hα/hα::β^A/β^A; "HbAA", "hemoglobin control") or (2) normal human γ and sickle cell human β-globin genes (hα/hα::β^S/β^S; "HbSS", "SCD"). Townes AA and SS mice were bred in house and maintained on a 14:10 light/dark cycle with *ad libitum* access to water and Teklad Global 16% Protein Rodent Diet chow (catalog #2916; irradiated). Equally sized cohorts of male and female mice were used in all experiments. Mice aged 8 -12 months were used in the FMT reversal experiments to capture the chronic phase of the disease phenotype; mice used in all other experiments were aged 3-9 months.

C57BL/6 "wild-type" mice. C57BL/6 mice were either bred in house or purchased from The Jackson Laboratory; purchased animals acclimated to housing facility for >7 days before experimental use. Purchased animals and animals bred in house were not intermixed but rather used in independent experiments. C57BL/6 mice were maintained in the same housing facility and provided the same diet as Townes mice. Equally sized cohorts of male and female C57BL/6 mice aged 8-26 weeks were used.

Akkermansia muciniphila

A. muciniphila was purchased through Amazon (produced by Pendulum Therapeutics, San Francisco, USA; lot A22201001 and 02220117). Live *A. muciniphila* was cultured from Pendulum probiotic capsules. To prepare the culture, a single capsule was transferred into a chamber with anaerobic conditions (5% H_2, 10% CO_2, 85% N_2). Prior to opening, the capsule surface was decontaminated by wiping thoroughly with 70% ethanol to minimize external microbial contamination. The contents of the capsule were aseptically transferred into 5mL of the pre-reduced BHI + 0.1% mucin medium and dissolved completely. The medium also contained 0.05% cysteine, 0.25 mg/ml resazurin, 0.12% hematin and 0.27M L-histidine (mucin medium adapted from: Derrien et al.[37], Miller and Hoskins[38]). The medium was reduced overnight in the chamber to ensure proper anaerobic growth. A 1:5 serial dilution in the same media was performed and incubated at 37 °C under strictly anaerobic conditions. Culture growth was measured at 24hr via optical density at 600nm (OD_{600}) and confirmed by 16S rRNA gene sequencing.

Please cite this article in press as: Brandow et al., Gut microbiota and metabolites drive chronic sickle cell disease pain in mice, Cell Host & Microbe (2025), https://doi.org/10.1016/j.chom.2025.08.012

Several glycerol starter culture tubes were made and frozen to culture *A. muciniphila* for the 7-day treatment paradigm. An overnight bacterial culture was grown to an OD600 of 0.7. A 500μL aliquot of the culture was harvested by centrifugation at 12,000rpm for 10min at room temperature. The supernatant was discarded, and the resulting cell pellet was resuspended in 50μL of 10% glycerol. The prepared starter culture was immediately frozen and stored at −80 °C for future use. One starter culture tube was used to inoculate 5mL of fresh medium for overnight growth. The culture was incubated for 22–24hr at 37 °C in the anaerobic chamber, after which cells were harvested. A 500μL aliquot of the overnight culture, normalized to a 0.7 OD each time, was centrifuged at 12,000rpm for 10 minutes at room temperature. The supernatant was discarded, and the cell pellet resuspended in 200μL of sterile saline. These cells were subsequently administered to mice.

Despite its poor growth performance on solid agar, robust cell yields were achieved in liquid cultures. To estimate cell concentration, OD_{600} values were calibrated against viable plate counts, establishing a correspondence of approximately 1.87×10^6 colony-forming units (CFU)/mL at $OD_{600} = 1$, as determined via spectrophotometric measurement (OD_{600}) using a calibrated Thermo Scientific GeneSys 30 spectrophotometer.

PLASMA AND STOOL SAMPLE DONORS

All patient and control sample collection procedures were approved by the IRB at Medical College of Wisconsin/Children's Wisconsin. Informed written consent was obtained from the participants' legal guardian and assent was obtained from the child when age appropriate.

Plasma analysis

Study participants included male and female children aged 7-19 years with SCD and healthy Black controls. Participant demographics are described in Table S3. Individuals with SCD were recruited during routine visits to the sickle cell clinic or when hospitalized for acute pain.

Stool analysis

Study participants included male and female individuals with SCD and healthy Black individuals without SCD who were both related and unrelated to those in the SCD group. Participant demographics are described in Table S4. Individuals with SCD were recruited and enrolled during routine visits to the SCD clinic.

Nodose ganglia tissue donors

All human tissue procurement procedures were approved by the IRB at the University of Texas at Dallas (UTD). Human nodose (samples 26 and 33) were procured from organ donors through a collaboration with the Southwest Transplant Alliance, while sample 343 was received from Anabios. All human nodose tissue was fresh frozen and stored in a -80°C freezer. Donor medical history was provided by the Southwest Transplant Alliance and Anabios and includes medical details from the donor's family members and hospital records. Donor demographics are provided in Table S5. Frozen nodose ganglia were gradually embedded in OCT in a cryomold by adding small volumes of OCT over dry ice to avoid thawing. Tissues were sectioned on a cryostat and used for histology and spatial transcriptomics. After sectioning, the remaining tissue blocks were wrapped in tin foil and then returned to the -80°C freezer for future use.

METHOD DETAILS

Animal treatments

Akkermansia muciniphila

A. muciniphila was administered to mice two different ways. Live *A. muciniphila* was administered to animals via oral gavage once a day for a total of 7 days at a dose of 9.35×10^5 CFU/mL (gavage volume was 200μL). Freeze-dried *A. muciniphila* was removed from commercial capsules, resuspended in sterile saline then administered to animals via oral gavage once a day for a total of 14 days at a dose of ~50 million AFU/mL (gavage volume was 200μL).

Fecal microbiota transplant

Animals received three fecal transplants (1 per day) over the course of three days. Fecal transplants were prepared by dissolving freshly collected fecal material in 1X phosphate buffered saline, pH 7.4 (1 fecal pellet/1 mL of PBS); a mixture of fecal pellets was collected from 2-5 separate, unrelated cages of mice then vigorously vortexed to aid in pellet dissolution. 200μL of resuspended fecal material was delivered via oral gavage to each recipient. Unless otherwise indicated, behavior was tested at the following fecal microbiota transplant (FMT) timepoints: "B" baseline, < 24hr before first FMT; "FMT", the morning of the third FMT day (*i.e.,* after 2 FMTs already performed); various timepoints following FMT cessation. In select experiments, FMT recipients were pre-treated with antibiotics to eliminate the existing microbiome (*i.e.,* make mice pseudo-germfree). Ampicillin (0.5g/L) was administered to animals in their drinking water for seven days. Fresh ampicillin-supplemented water was provided every other day, then replaced with normal drinking water on day 8. Twenty-four hours following ampicillin treatment cessation, animals began FMT paradigm. Experiments including an "amp" testing timepoint were performed on day 3 or 4 following the start of ampicillin treatment.

Please cite this article in press as: Brandow et al., Gut microbiota and metabolites drive chronic sickle cell disease pain in mice, Cell Host & Microbe (2025), https://doi.org/10.1016/j.chom.2025.08.012

Bilirubin treatment

Bilirubin was dissolved in vehicle containing 10% DMSO, 40% PEG 400, 5% Tween 80, 45% saline immediately prior to use. Bilirubin or vehicle solution (200μL) was administered via oral gavage.

A23 treatment

A23 is a selective TRPM2 inhibitor.[17,18] A23 was dissolved in vehicle containing 5% DMSO, 5% Kolliphor, 90% saline immediately prior to use. A23 or vehicle solution was administered via oral gavage 30 minutes prior to behavior assessment.

Hydroxyurea treatment

Hydroxyurea is a disease modifying treatment prescribed to individuals born with SCD. To model clinical practice, Townes HbSS (SCD) mice started hydroxyurea treatment on postnatal day 1 (50 mg/kg of dam body weight, dissolved in cage drinking water) and remained on this treatment for the rest of their lives (25 mg/kg following weaning, dissolved in cage drinking water). Hydroxyurea solution was changed every other day and adjusted for collective weight of animals in a given cage. Fecal material was collected from 3 month old HU-treated SCD mice.

Subdiaphragmatic vagotomy

Briefly, once animals were anesthetized with isoflurane, a longitudinal incision was made through the skin and underlying fascia from the umbilicus region of the abdomen to just below the xiphoid process. A second incision of the same size was made in the underlying abdominal cavity wall. Using a sterile cotton-tipped swab, the internal organs were gently moved in order to visualize where the vagus nerve passes through the diaphragm. In vagotomized animals, the trunks of the left and right vagus nerve were cut immediately before ascending through the diaphragm; in sham animals, the nerve trunks were visualized, then the visceral organs were returned to their original positions. Vagotomized animals also received pyloroplasty to prevent excessive stomach distension. A longitudinal cut was made through the pylorus muscle; this cut was then sutured horizontally to allow for continual stomach emptying. Both the abdominal cavity and skin incisions were secured with two to three sutures. C57BL/6 mice were vagotomized nine days prior to bilirubin treatment. Behaviors tests were performed in SCD and hemoglobin control mice 3 days following vagotomy.

Behavior tests

Animals were habituated to testing chambers/apparatus for >1.5hr prior to all behavior tests. The experimenter, who was blinded to treatment and/or genotype, remained in the behavior room for an additional 30min prior to the start of behavior testing to allow for olfactory signal habituation.

von Frey punctate mechanical sensitivity testing

Animals were placed into 10 x 10 x 15cm^3 Plexiglass chambers on a raised 0.7cm^2 wire platform. Calibrated monofilaments were delivered through the wire platform and applied to the plantar surface of each hindpaw following the up-down method[39]; the 50% withdrawal threshold of each paw was calculated then averaged between paws.[40] Toe flaring was not considered a "withdrawal".

Plantar dry ice cold sensitivity testing

Animals were placed into the aforementioned Plexiglass chambers on a raised 1/8" or 1/4" thick glass platform; note that the same thickness of glass was used for all animals in the same experiment. Powdered dry ice was applied to the glass underneath the plantar surface of each hindpaw as previously described.[41] The withdrawal latency of each paw was assessed five times, then averaged between paws.

Noxious punctate mechanical sensitivity testing

Animals were placed into the aforementioned Plexiglass chambers on a raised 0.7cm^2 wire platform. A 25Ga needle was applied to the center of the plantar surface of each hindpaw 10 times; response frequency and characterization were reported. Responses were characterized as follows: null (no paw withdrawal), normal (paw removed from wire mesh then immediately returned), or nocifensive (paw withdrawal accompanied by flicking, licking, biting, hovering of paw above mesh, slamming of paw back onto mesh surface).

Dynamic light touch mechanical sensitivity testing

Animals were placed into the aforementioned Plexiglass chambers on a raised 0.7cm^2 wire platform. A fine, liner paintbrush (Princeton Good Synthetic Golden Taklon brush, size 2) was dragged – from heel to toes – across the glabrous surface of each hindpaw 10 times; response frequency and characterization was reported in a manner identical to needle testing.

Radiant heat sensitivity testing

Animals were placed into the aforementioned Plexiglass chambers on a raised 1/4" glass platform. A focal radiant heat source was applied to the glass immediately underneath the plantar surface of each hindpaw as previously described.[42] The withdrawal latency of each paw was assessed five times, then averaged between paws.

Sample preparation for 16S ribosomal RNA gene sequencing

Mouse fecal material

Animals were individually placed into glass beakers for fecal collection. For FMT-related sequencing, fecal material was collected from the same cohort of C57BL/6 mice at the following time points: < 24hr prior to start of antibiotic administration (B: baseline), 4 days following the start of antibiotic administration (amp: ampicillin), and < 24hr following the final of three FMTs. For bilirubin-related sequencing, fecal material was collected from Townes SS mice and the same cohort of Townes AA mice <24hr before bilirubin administration, then again 24hr and 5 days following oral administration of bilirubin (200 μM). Fecal material was collected immediately following excretion, placed into 0.5-1mL of RNAlater, then frozen on dry ice. Fecal DNA was extracted using the Qiagen DNeasy Powerlyzer Powersoil Kit and the modified protocol described by Kommineni et al.[43] The V3/V4 region (341F – 806R) of the

Please cite this article in press as: Brandow et al., Gut microbiota and metabolites drive chronic sickle cell disease pain in mice, Cell Host & Microbe (2025), https://doi.org/10.1016/j.chom.2025.08.012

16S rRNA gene was amplified via PCR and sequenced on the MiSeq platform (Illumina) using 2x300bp read technology at the University of Wisconsin-Madison Biotechnology Center, Madison, Wisconsin.

Patient fecal material

Stool samples were self-collected by participants during baseline state of health, defined as the absence of an acute care visit for pain or another SCD complication for at least two weeks, via supplied kits, preserved in RNAlater, and sent to the laboratory via FedEx delivery from patient or pickup by research coordinator and stored in -80°C freezer. Microbial DNA was extracted with PowerSoil® DNA Isolation kit (MoBio) following the manufacturer's guidelines. The 16S DNA V3-V4 region amplicons (single index) were produced by PCR. Deidentified samples were and sequenced on the MiSeq platform (Illumina) using the 2x300bp protocol yielding pair-end reads that overlap by ~464 bps.[44]

16S ribosomal RNA gene sequencing

QIIME2 (v. 2022.8, mouse; v. 2024.5, human) was used to analyze the paired-end 16S DNA sequencing reads.[36] Sequences were imported and summarized to check quality. Cutadapt was used to trim primers from the reads.[45] Representative sequences were chosen using DADA2, which also removes chimeric sequences.[46] The representative sequences were then aligned,[47] masked for hypervariable regions,[48] and phylogenetic trees were produced.[49] A classifier was generated to assign taxonomy to the reads using the 99% similarity files of the SILVA v. 138 and the 341-806 region (V3/V4) of the 16S gene.[50,51] Taxonomy was assigned to the feature table to make taxonomy bar plots and to generate relative abundance tables.

Diversity metrics were run using the *core-metrics-phylogenetic* command of QIIME2. Alpha and beta diversity were analyzed using their respective commands, *alpha/beta-group-significance*.[52–54] Alpha diversity metrics used a Kruskal-Wallis test to test for significance, while beta diversity metrics used a PERMANOVA test; both types of metrics used Benjamini-Hochberg multiple comparison tests. Principal Coordinate Analysis (PCoA) plots were examined using EMPeror[55,56] and finalized figures were made using the qiime2R package and ggplots2 in R.[57–59] Differentially abundant taxonomy was calculated between two groups using LEfSe (Linear discriminate analysis (LDA) effect size) using default parameters except for -w being set to 1, as there were no subgroups to test.[60] MaAsLin2 was used to determine differentially abundant taxa when multiple variables were being analyzed.[61]

To look at the abundance of putative BilR producing bacteria the human-based abundance table was filtered to retain only genera that match the Table S1 from Hall et al.,[13] of which there were 30. The Hall table was then further used to label each genus in the matched abundance table as short, long, or mixed BilR length. Mixed BilR length label was given if there was a mix of short and long labels for the species belonging to the genus in our table. The resulting table was run through MaAsLin2 to determine genera that are differentially abundant based on BilR length.[61]

Immunofluorescent staining

MUC2 staining of colon

For analysis of MUC2 and goblet cells in colonic mucosa, colon tissue was mounted with a *swiss-roll* technique as described[62] and sliced at 30μm on a cryostat. Colon sections were stained with a rabbit pAb to MUC2 (1:200). After washing several times, incubation with AlexaFluor 488-conjugated goat anti-rabbit secondary antibody and Hoechst 33342 (1:1000) was performed. All sections were mounted with ProLong Gold antifade reagent and imaged with FV-4000 (Olympus; UPlanXApo 20X/ 0.80/0.17/OFN26.5; UPlanApo 60X/1.50 Oil HR/0.13-0.19/OFN22) confocal microscope. All samples were processed and analyzed in a blinded fashion using Image-J (http://imagej.nih.gov).

For analysis of MUC2, 6 random 20X fields were analyzed per animal. Positive MUC2 staining was segmented using a manually determined threshold value based on visual distinction between positive and background areas. The percentage positive area within each annotated section was calculated by taking the number of segmented pixels in each map divided by the total number of pixels in the annotation section. For analysis of goblet cells, 6 distal 60X (oil immersion) fields were taken per animal. Goblet cells number per crypt were reported as previously described.[63]

pERK1/2 staining in NTS

Brain sections (30μm thick) containing the nucleus of solitary tract (NTS) were cut on a cryostat. For pERK analysis, NTS sections were immunostained with rabbit anti-pERK1/2 (p-P44/42; 1:200) and mouse anti-NeuN (1:300) antibodies. After washing several times, NTS sections were incubated with AlexaFluor-488 goat anti-rabbit IgG (H+L) (1:500) and Alexa Fluor 647 goat anti-mouse IgG (1:500) secondary antibodies and Hoechst 33342 (1:1000, H3570, Invitrogen). All sections were mounted with ProLong Gold antifade reagent (Invitrogen, Cat: P36930) and imaged with FV-4000 (Olympus; UPlanXApo 20X/ 0.80/0.17/OFN26.5) confocal microscope. For analysis of pERK1/2, 5–6 20X NTS sections per animal were analyzed blinded with Image-J (http://imagej.nih.gov). The number of positive pERK1/2 cells per area as well as double positive pERK1/2 and NeuN cells (pERK1/2 positive neurons) per area was reported as previously described.[64]

Gut permeability

Gut permeability was assessed using FITC-dextran. Twenty-four hours following the last of three FMTs, mice began an overnight fasting period. The following morning, Fluorescein isothiocyanate-dextran (FITC-dextran, dissolved to concentration of 100 mg/mL in 1X phosphate buffered saline, pH 7.4) was orally administered to mice at a concentration of 44mg/100g body weight. Four

Please cite this article in press as: Brandow et al., Gut microbiota and metabolites drive chronic sickle cell disease pain in mice, Cell Host & Microbe (2025), https://doi.org/10.1016/j.chom.2025.08.012

hour later, trunk blood was collected via cardiac puncture. Blood was stored in the dark on ice, then centrifuged to separate plasma. Plasma was diluted 1:1 with 1X PBS, the mean fluorescence of each sample was detected on a 485nm plate reader and circulating FITC-dextran levels were extrapolated from a standard curve.

Bacterial translocation assessment

Twenty-four hours following the last of three FMTs, mesenteric lymph nodes were collected from FMT recipient mice. Tissues were weighed and homogenized in 1X PBS (10μL of PBS for every 1mg of tissue). Serial dilutions of homogenate were grown on Trypticase soy agar, 5% sheep blood plates at 37°C; colony forming units were counted 48hr later.

Probiotic DNA extraction, amplification, and species confirmation

Bacterial DNA was extracted from commercially available *A. muciniphila* pills and freshly cultured *Staphylococcus aureus* (gifted by Xintong Dong) using the Qiagen DNeasy Powerlyzer Powersoil Kit and the modified protocol described by Kommineni et al.[43] Quantitative real time PCR was run using Thermo Scientific™ DreamTaq™ Hot Start Green DNA Polymerase, universal bacteria primers, and *Akkermansia* primers. The Bio-Rad T100 Thermal Cycler settings for PCR were as follows: (1) 94°C for 8 minutes; (2) 94°C for 30 seconds; (3) 55°C for 30 seconds; (4) 72°C for 30 seconds; (5) GO TO step 2 (34X). The amplified samples were then loaded onto a 1% agarose gel in the Bio-Rad Sub-Cell GT Electrophoresis Chamber and allowed to run for 45 minutes at 100V to allow for adequate separation of bands. Visualization was accomplished using the Bio-Rad ChemiDoc imaging system. In addition to confirming *A. muciniphila* presence in probiotic capsules via qPCR, the 16S rRNA gene was also sequenced and identified as *A. muciniphila*.

Quantitative real-time PCR of gap junction genes

Total RNA was extracted from homogenized colon segments using the Qiagen RNeasy Plus Universal Mini Kit according to the manufacturer's protocol. RNA concentration and purity was determined using the Thermo Scientific™ Invitrogen™ Nanodrop ™ One Spectrophotometer. RNA was reverse transcribed into cDNA using the Qiagen QuantiTect Reverse Transcription Kit. Quantification of select gap junction gene expression was performed using PowerUp™ SYBR™ Green Master Mix in the CFX Duet Real-Time PCR System (Bio-Rad) with the complementary CFX Maestro Software. Occludin1, Claudin2, Mucin2, and 18S primers were purchased from Integrated DNA Technologies in LabReady (100 μM in IDTE, pH 8.0) formulation. Initial activation of enzymes was induced through a 95°C hold for 3 minutes. This was followed by 40 cycles of a 2-step PCR of 95°C for 10 seconds and 60°C for 30 seconds. Readings were completed in triplicates and the delta delta Ct ($2^{-\Delta\Delta Ct}$) method was used to calculate mRNA fold change values. The housekeeping gene 18S was used to normalize values, which were then made relative to the average delta Ct of the HbAA (control) group.

Nodose/jugular ganglia calcium imaging and electrophysiology

Nodose/jugular ganglia neuronal isolation and culture

Bilateral nodose/jugular ganglia (NJG; contained within the same strucutre in mouse) were isolated from naïve C57BL/6 wildtype mice, or from FMT or bilirubin treated animals (tissue was collected approximately 24hr following the final FMT or 24hr following 200μM oral bilirubin administration). After isoflurane anesthesia and cervical dislocation, an incision was made in the lateral aspect of the neck at the level of the hyoid bone. Following removal of the sternocleidomastoid and masseter muscles, the facial (VII), glossopharyngeal (IX), vagus (X), accessory (XI), and hypoglossal (XII) cranial nerves were visible. After identifying the vagus nerve by observing its parallel orientation to the carotid artery, the nerve trunk was traced in a rostral fashion until it entered the skull at the jugular foramen; the NJG appeared as white swellings within each jugular foramen. Both NJG were excised, incubated in DMEM/Ham's F12 medium containing 10mg/mL collagenase for 40min at 37°C, then 0.5% trypsin for 45min at 37°C. Following trypsin neutralization in 3% heat-inactivated horse serum, NJG were mechanically dissociated then plated on laminin-coated glass coverslips. Neurons were incubated overnight at 37°C, 5% CO_2 in DMEM/Ham's F12 medium supplemented with 10% heat-inactivated horse serum, 2mM L-glutamine, 1% glucose, 100units/mL penicillin, and 100μg/mL streptomycin. Patch clamp electrophysiology or calcium imaging was performed on neurons 12–24hr following tissue isolation.

Whole-cell patch clamp electrophysiology

Patch clamp recordings of isolated NJG neurons were performed following overnight culture. Neurons were visualized using a Nikon Eclipse TE200 inverted microscope, and coverslips were continuously superfused with extracellular buffer (140mM NaCl, 2.8mM KCl, 2mM $CaCl_2$, 1mM $MgCl_2$, 10mM HEPES, 10mM glucose, and 8.8mM sucrose, pH 7.4 ± 0.02 and 310 ± 3mOsm). Borosillicate glass pipettes (2.4 to 4.2MΩ) filled with internal solution (135mM KCl, 4.1mM $MgCl_2$, 2mM EGTA, 0.2 mM NaGTP, 2.5mM $ATPNa_2$, and 10mM HEPES, pH 7.2 ± 0.02 and 290 ± 2mOsm) were pulled using a Sutter Instruments P87 pipette puller and used to perform patch clamp recordings. Series resistance was maintained at <10MΩ and compensated at 60%. Neuronal capacitance was fully compensated and continuously monitored to ensure stable recording conditions.

Whole-cell recordings were obtained using a HEKA EPC10 amplifier and Patchmaster software. Data were collected from neurons with a resting membrane potential (RMP) $\leq$ -40mV. In FMT recordings, neurons were held at -70mV; in bilirubin recordings, neurons were held at RMP. Measures of intrinsic excitability were recorded using the following protocols: (1) Voltage-current (*V-I*) relations were obtained using 20 sweeps of 500ms ascending current pulses (5pA stepwise increase from holding current). The plateau voltage deflection was plotted against current amplitude, and input resistance was determined from the slope of the *V-I* plot where voltage sweeps did not exhibit active conductance. (2) Action potential (AP) properties were measured using an ascending series of

Please cite this article in press as: Brandow et al., Gut microbiota and metabolites drive chronic sickle cell disease pain in mice, Cell Host & Microbe (2025), https://doi.org/10.1016/j.chom.2025.08.012

5ms depolarizing current pulses. Rheobase was defined as the first current to elicit a single spike. AP threshold was determined from a derivative function, where dV/dt first exceeded 28mV/ms. AP amplitude was determined relative to AP threshold, and AP half-width was measured as the width at half of the AP amplitude. (3) A series of depolarizing current steps were used to elicit action potentials. In FMT recordings, nine 500ms (range: rheobase to 1600pA above rheobase; 200pA increments, 20s intervals) were used; in bilirubin recordings, seventeen 500ms (range: rheobase to 400pA above rheobase; 25pA increments, 20s intervals) were used. (4) The post-burst afterhyperpolarization (AHP; avg. of 3 sweeps at 20s intervals) was examined using a 50Hz burst of 10 spikes evoked by a 2ms suprathreshold current pulse. The average AHP amplitude during the first 150ms following current offset was used to determine the medium AHP (mAHP), while the AHP amplitude at 1s following current offset was used to determine the slow AHP (sAHP). Recorded neurons were classified as either single-fire (firing only 1 AP regardless of current magnitude) or multiple-fire (firing more than 1 AP at suprathreshold currents). Spontaneous activity was recorded in current clamp mode for 2min after voltage-current relationships were assessed and prior to depolarizing current injection steps.

NJG neuronal calcium imaging

Calcium imaging of isolated NJG neurons from naïve, C57BL/6 mice was performed following overnight culture. Neurons were loaded with the dual-wavelength, ratiometic calcium indicator dye, Fura-2-AM (2.5μg/mL in 2% bovine serum albumin) for 45min, then washed with extracellular buffer (150mM NaCl, 5.6mM KCl, 2mM $CaCl_2$, 1mM $MgCl_2$, 1mM HEPES, 8 mM glucose, pH 7.4 ± 0.02 and 320 ± 3mOsm) for 30min. Coverslips were mounted onto a Nikon Eclipse TE200 inverted microscope, and superfused with extracellular buffer at a rate of 6 mL/min. Cells were superfused with bilirubin (2, 20, or 200μM) prepared in 10% DMSO, 40% PEG 400, 5% Tween 80, 45% PBS for 30s, then 50mM KCl for 30s. Bilirubin was prepared immediately before use and protected from light exposure. Fluorescence images were captured at 340 and 380nm using NIS Elements Software. Responders were cells that exhibited a $\geq$ 20% increase in 340/380nm ratio from baseline during the bilirubin application and prior to 50mM KCl exposure. Null responders were cells that only exhibited a $\geq$ 20% increase in 340/380nm ratio from baseline during 50mM KCl exposure. For A23 experiments, cells were incubated with A23 (10 or 100μM; dissolved in 0.10% DMSO vehicle) or vehicle for 2min prior to bilirubin application.

Metabolite screens

Mouse fecal material

Fecal metabolite screening was performed by Metabolon (Morrisville, NC). Briefly, fecal material was collected using the methods described for 16S sequencing. Upon excretion, fecal material was immediately collected and transferred to an empty, pre-chilled tube. Samples were frozen on dry ice and shipped to Metabolon. For unbiased metabolomic analyses, samples were prepared using the automated MicroLab STAR system (Hamilton Company). Sample compounds were measured using a Waters ACQUITY ultra-performance liquid chromatography and Thermo Scientific Q-Exactive high resolution/accurate mass spectrometer interfaced with a heated electrospray ionization (HESI-II) source and Orbitrap mass analyzer operated at 35,000 mass resolution. Compounds were identified by comparison to purified standards, and relative metabolite concentrations were calculated using Metabolon hardware and software. For short chain fatty acid (SCFA) analysis, fecal samples were homogenized, proteins were precipitated via dissolution in organic solvents, then remaining supernatant was injected into an Agilent 1290/SCIEX QTRAP 5500 LC MS/MS system equipped with a C18 reversed phase UHPLC column. LC-MS/MS data was processed using SCIEX OS-MQ software; sample values were compared to internal and calibration standards.

Bilirubin levels in mouse fecal material

Targeted assessment of bilirubin levels in hydroxyurea and vehicle-treated sickle cell disease mouse feces was completed using the Bilirubin Assay Kit. Fecal material was collected using the methods described for 16S sequencing then immediately suspended in sterile water (1mg feces per 10μL of water). Samples were vortexed, left to sit at room temperature for 10min, then centrifuged for 30s. Bilirubin was measured in supernatant according to manufacturer directions.

Patient plasma

Plasma was collected during baseline state of health, defined as the absence of an acute care visit for pain or another sickle cell disease complication for at least two weeks, or during hospitalization for acute pain. Plasma was collected by peripheral venipuncture, immediately centrifuged and stored in 500μl aliquots in -80°C freezer until use. De-identified patient samples were sent to Metabolon (Morrisville, NC) for unbiased metabolomic screen.

RNAscope *in situ* hybridization

RNAscope *in situ* hybridization multiplex version 2 (Advanced Cell Diagnostics) was performed using the manufacturer's fresh frozen protocol and as previously described.[65]

Human nodose ganglia (samples 33, 26, and 343) were sectioned at 20μm onto SuperFrost Plus charged slides. Sections were only briefly thawed in order to adhere to the slide but were immediately returned to the -20°C cryostat chamber until completion of sectioning. The slides were removed from the cryostat, thawed for 1min at 37°C, and then immediately immersed in 10% formalin for 15min. The tissues were then sequentially dehydrated in 50% ethanol (5min), 70% ethanol (5min), and two times in 100% ethanol (5min) at room temperature. The slides were air dried briefly and then boundaries were drawn around each section using a hydrophobic pen. Once the hydrophobic boundaries had dried, the slides were immediately processed for RNAscope *in situ* hybridization.

Hydrogen peroxide was applied to each section until fully covered then incubated for 10min at room temperature. The slides were then washed in distilled water and then incubated one at a time in protease III reagent for 10s at room temperature. The protease

Please cite this article in press as: Brandow et al., Gut microbiota and metabolites drive chronic sickle cell disease pain in mice, Cell Host & Microbe (2025), https://doi.org/10.1016/j.chom.2025.08.012

incubation time was optimized as recommended by ACD for the tissue and specific lot of protease reagent. Slides were washed briefly in 1X phosphate buffered saline (PBS, pH 7.4) at room temperature. Each slide was then placed in a prewarmed humidity control tray containing damp filter paper and a mixture (50:1:1 dilution) of *TRPM2*, *PHOX2B*, and *TRPV1* probes was pipetted onto each section until fully covered. This was performed one slide at a time to avoid liquid evaporation and section drying. The humidity control tray containing the slides was placed in a HybEZ oven for 2hr at 40°C. Following probe incubation, the slides were washed two times in 1X RNAscope wash buffer and then placed in 5X SSC buffer over night at room temperature.

The following morning, the slides were washed two times in 1X RNAscope wash buffer and placed in the 40°C oven for 30min after submersion in AMP-1 reagent. Washes and amplification were repeated using AMP-2 and AMP-3 reagents with a 30min and 15min incubation period, respectively. HRP-C1 reagent was applied to all sections and then incubated in the oven at 40°C for 15min. The slides were then washed in 1X RNAscope wash buffer. TSA Plus Akoya Dyes in Fluorescin, Cyanine-3, and Cyanine-5 were prepared at 1:1000 in TSA buffer. The Akoya dye assigned to Channel 1 probe was applied to each section until fully covered and incubated for 30min in the 40°C oven. The slides were washed and then covered in HRP blocker for 15min at 40°C. The slides were washed again and then the same steps were repeated using HRP-C2 and HRP-C3 reagents with their assigned Akoya dye. DAPI was applied to each section for 1min at room temperature and then washed in 1X PBS (pH 7.4) before being washed, air dried, and cover-slipped with Prolong Gold Antifade mounting medium.

A positive and negative control was run on a single section from each nodose sample in the same RNAscope experiment. The positive control probe cocktail contains probes for high, medium and low-expressing mRNAs that are present in all cells (ubiquitin C > Peptidyl-prolyl cis-trans isomerase B > DNA-directed RNA polymerase II subunit RPB1) and allows us to gauge tissue quality and experiment conditions. All tissues showed robust signal for all 3 positive control probes. A negative control probe against the bacterial DapB gene was used to check for lipofuscin and background label.

Nodose sections were imaged on an FV3000 confocal microscope (Evident Scientific) at 20X or 40X magnification. The acquisition parameters were set based on guidelines for the FV3000 provided by Evident Scientific. The raw image files were analyzed in CellSens (Olympus; v1.18) by counting all neurons with a minimum of 3 puncta. Graphs were generated using GraphPad Prism version 10.0.2. The True black lipofuscin quencher (used in immunofluorescence) is not compatible with RNAscope. Large globular structures and/or signals that auto fluoresced in all channels (particularly brightest in 488 and 555 wavelengths) was considered background lipofuscin and was not analyzed. Aside from adjusting brightness/contrast, we performed no digital image processing to subtract background.

Human nodose ganglia spatial transcriptomics

Spatial RNA-sequencing was conducted with the 10x Genomics VISIUM assay using the tissue optimization and spatial gene expression protocols provided by 10x Genomics and similar to those that we previously used for human dorsal root ganglia.[66]

After determination of optimal permeabilization time (24min), 8 human nodose tissue sections from 3 different donors were each mounted onto a frame of the same VISIUM slide. One human nodose sample did not pass quality checks (low neuronal barcode count) and was removed from the analysis. Hematoxylin and eosin staining was used to visualize the tissue, and imaging was done with an Olympus vs120 slide scanner. mRNA library preparation was performed with the Spatial 3′ v1 kit and sequenced with the Illumina NextSeq 2000 by Genome Center at UTD.

The 10x Genomics SpaceRanger pipeline (version 1.1.0) was used to process raw sequencing files and generate count matrices of gene expression per VISIUM barcode in each sample. Barcodes that overlapped neurons were identified using the 10x Genomics Loupe Browser. Gene expression analysis of neuronal barcodes was done with R (version 4.3.3). The ggplot2 package (version 3.5.1) was used to visualize gene expression in human nodose neurons per sample. It was also used to visualize gene expression per cluster of a single-cell mouse nodose dataset published by Kupari et al.[23] The raw and processed sequencing files from human nodose samples are available on dbGaP, and processed sequencing files are available on SPARC (DOI: 10.26275/6vkg-lpxp).

QUANTIFICATION AND STATISTICAL ANALYSIS

Individual data points were presented whenever possible. All other data are presented as group means ± SEM. Unless otherwise described, data were analyzed using GraphPad Prism 10; results were considered statistically significant when $p < 0.05$. Data from each sex was independently analyzed then combined if no sex difference was observed. Sex differences were only observed in heat sensitivity following SCD FMT.

Cell Host & Microbe, Volume *33*

Supplemental information

Gut microbiota and metabolites drive chronic sickle cell disease pain in mice

Amanda M. Brandow, Samantha N. Atkinson, Zulmary Manjarres, Vanessa L. Ehlers, McKenna L. Pratt, Iti Mehta, Sruthi Mudunuri, Aishwarya Kappagantu, Stephanie I. Shiers, Khadijah Mazhar, Mackenzie A. Simms, Sahar Alhendi, Anagha Sheshadri, Anna M. Cervantes, Jeffrey C. Reese, Diana Tavares-Ferreira, Ishwarya Sankaranarayanan, Mandee K. Schaub, Tyler B. Waltz, Michael Hayward, Dianise M. Rodríguez García, Gregory Dussor, Nita H. Salzman, Kelli L. Palmer, Cheryl L. Stucky, Theodore J. Price, and Katelyn E. Sadler

Supplemental Items

Supplemental figures

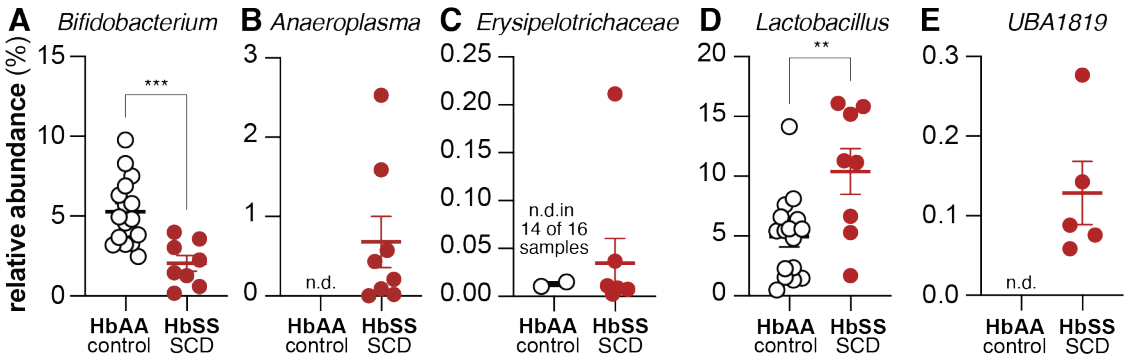

Figure S1: Differentially abundant bacteria in SCD and hemoglobin control fecal material, Related to Figure 1. MaAsLin2 multivariate analysis of 16S rDNA sequencing of Townes SS (SCD) and Townes AA (control) fecal material revealed significant differences in the relative abundance of the following bacteria: (**A**) *Bifidobacterium*, (**B**) *Anaeroplasma*, (**C**) *Erysipelotrichaceae*, (**D**) *Lactobacillus*, (**E**) *UBA1819*; Kruskal-Wallis test $^{**}P<0.01$, $^{***}P<0.001$.

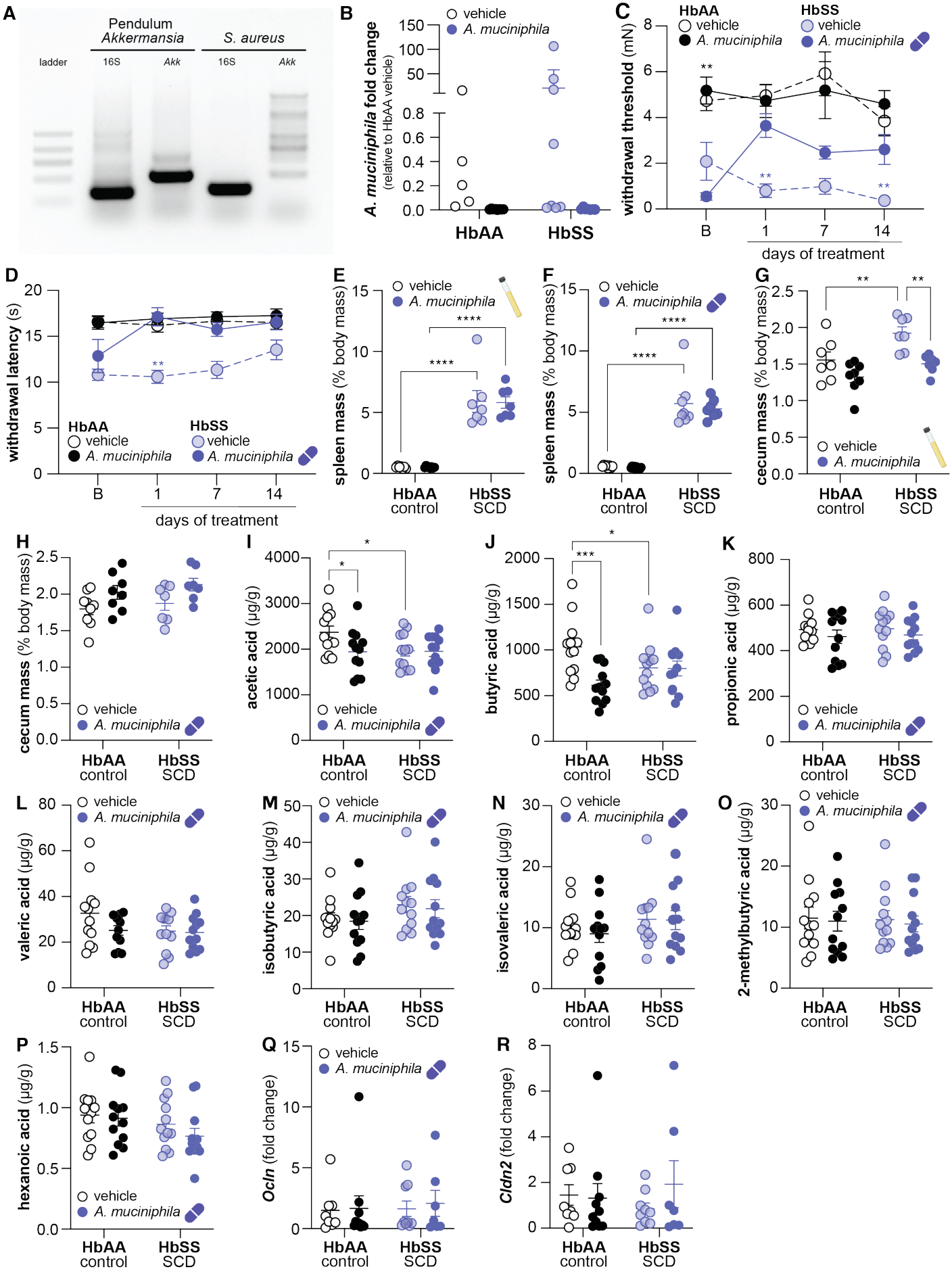
A
Pendulum
Akkermansia
S. aureus
ladder
16S
Akk
16S
Akk
B
vehicle
A. muciniphila
A. muciniphila fold change
(relative to HbAA vehicle)
HbAA
HbSS
C
HbAA
vehicle
A. muciniphila
HbSS
vehicle
A. muciniphila
withdrawal threshold (mN)
B
1
7
14
days of treatment
D
withdrawal latency (s)
HbAA
vehicle
A. muciniphila
HbSS
vehicle
A. muciniphila
B
1
7
14
days of treatment
E
vehicle
A. muciniphila
spleen mass (% body mass)
HbAA
control
HbSS
SCD
F
vehicle
A. muciniphila
spleen mass (% body mass)
HbAA
control
HbSS
SCD
G
cecum mass (% body mass)
vehicle
A. muciniphila
HbAA
control
HbSS
SCD
H
cecum mass (% body mass)
vehicle
A. muciniphila
HbAA
control
HbSS
SCD
I
acetic acid (µg/g)
vehicle
A. muciniphila
HbAA
control
HbSS
SCD
J
butyric acid (µg/g)
HbAA
control
HbSS
SCD
K
propionic acid (µg/g)
vehicle
A. muciniphila
HbAA
control
HbSS
SCD
L
valeric acid (µg/g)
vehicle
A. muciniphila
HbAA
control
HbSS
SCD
M
isobutyric acid (µg/g)
vehicle
A. muciniphila
HbAA
control
HbSS
SCD
N
isovaleric acid (µg/g)
vehicle
A. muciniphila
HbAA
control
HbSS
SCD
O
2-methylbutyric acid (µg/g)
vehicle
A. muciniphila
HbAA
control
HbSS
SCD
P
hexanoic acid (µg/g)
vehicle
A. muciniphila
HbAA
control
HbSS
SCD
Q
Ocln (fold change)
vehicle
A. muciniphila
HbAA
control
HbSS
SCD
R
Cldn2 (fold change)
HbAA
control
HbSS
SCD

Figure S2: *Akkermansia muciniphila* effects on SCD and hemoglobin control mice, Related to Figure 1. (**A**) Agarose gel electrophoresis confirmation of PCR product following amplification of a universal 16S DNA sequence and *Akkermansia* (*Akk*) specific DNA sequence. (**B**) *A. muciniphila* relative abundance in fecal samples from hemoglobin control (HbAA) or SCD (HbSS) mice collected on day 7 of vehicle or *A. muciniphila* treatment. Decreased *A. muciniphila* in probiotic-treated mice may indicate successful colonization. (**C**) Hindpaw mechanical withdrawal thresholds of Townes HbAA (control) and HbSS (SCD) mice prior to and during supplementation with freeze-dried *A. muciniphila*; 3-way RM ANOVA main effects of genotype $P<0.0001$, time x treatment interaction $P<0.05$, and time x treatment x genotype interaction $P<0.01$, corrected Fisher's exact post-hoc comparisons $^{**}P<0.01$ (black: vehicle control vs. SCD, purple: SCD vehicle vs. *Akkermansia*), B: baseline, $N=8$-10. (**C**) Hindpaw withdrawal latency to dry ice application of Townes HbAA and HbSS mice prior to and during supplementation with freeze-dried *A. muciniphila*; 3-way RM ANOVA main effects of time $P<0.05$, genotype $P<0.0001$, treatment $P<0.0001$, and genotype x treatment interaction $P<0.0001$, corrected Fisher's exact post-hoc comparisons $^{**}P<0.01$ (purple: SCD vehicle vs. *Akkermansia*), B: baseline, $N=8$-10. Relative spleen size following (**E**) live or (**F**) freeze-dried *A. muciniphila* treatment. Relative cecum size following (**G**) live or (**H**) freeze-dried *A. muciniphila* treatment. LC-MS/MS quantification of (**I**) acetic acid, (**J**) butyric acid, (**K**) propionic acid, (**L**) valeric acid, (**M**) isobutyric acid, (**N**) isovaleric acid, (**O**) 2-methylbutyric acid, and (**P**) hexanoic acid in fecal samples collected from SCD and hemoglobin control mice following 14 days of vehicle of *A. muciniphila* treatment. Quantitative real-time PCR analysis of (**Q**) Ocln (Occludin) and (**R**) Cldn2 (Claudin-2) gene expression in distal colon isolated from SCD and hemoglobin control mice following 14 days of vehicle or *A. muciniphila* treatment. Fold change relative to HbAA vehicle control group.

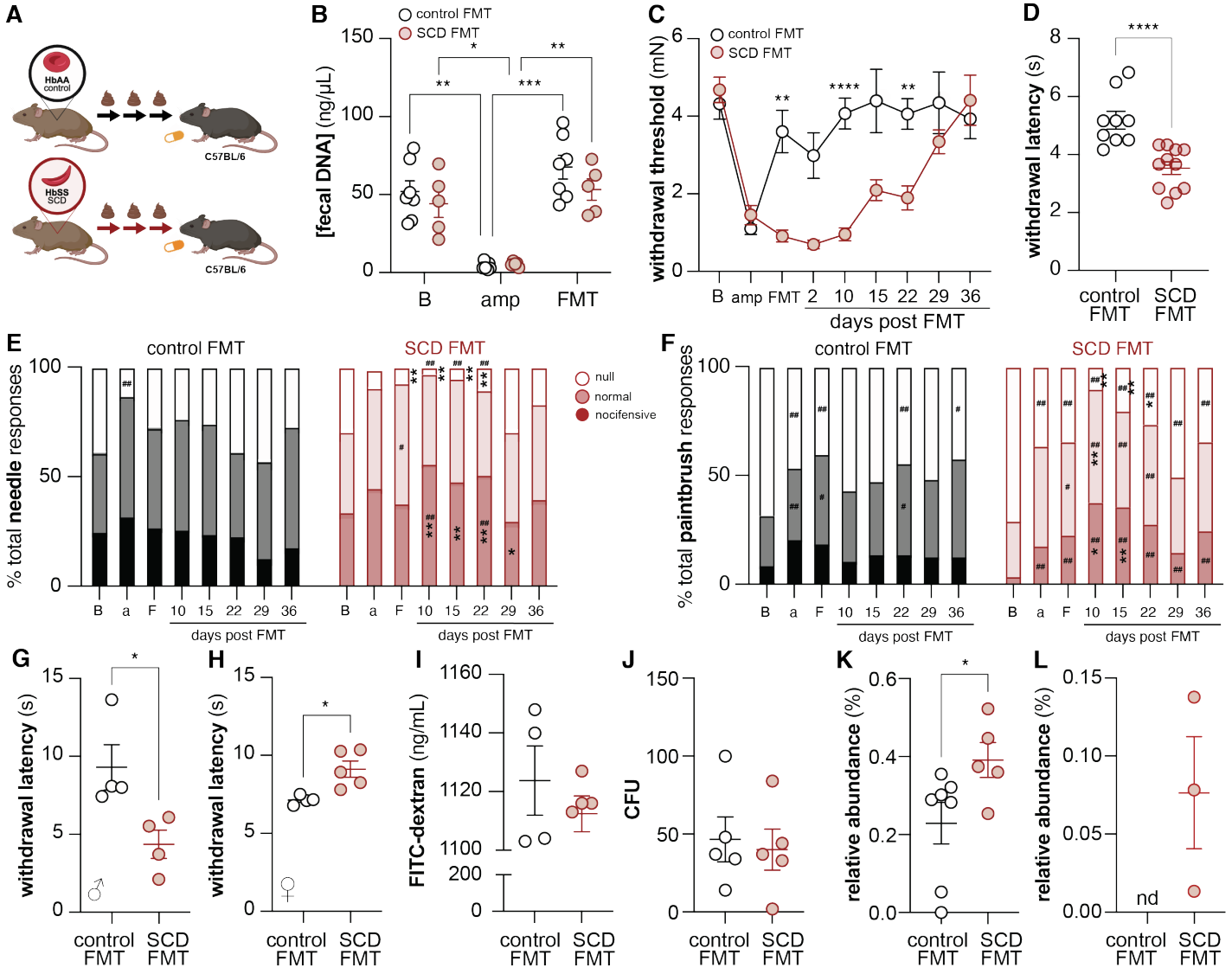

Figure S3: SCD fecal microbiota transplant (FMT) induces pain in antibiotic pre-treated recipients, Related to Figure 2. (**A**) Three-day FMT paradigm design for antibiotic pre-treated C57BL/6 mice. (**B**) DNA concentration in fecal samples collected from recipient mice throughout FMT paradigm. (**C**) Hindpaw mechanical withdrawal thresholds of C57BL/6 mice during FMT paradigm. C57BL/6 mice received FMT from HbAA (control) or HbSS (SCD) mice after 7 days of ampicillin treatment; *N*=15-17, B: baseline, amp: day 3 of ampicillin treatment. (**D**) Hindpaw withdrawal latency of C57BL/6 mice to dry ice application at FMT timepoint; unpaired t-test ****P<0.0001. (**E**) Noxious needle responses of hemoglobin control and SCD FMT recipients throughout FMT paradigm; Fisher's exact post hoc comparisons: *P<0.05 control vs. SCD, **P<0.01, control vs. SCD, $^{\#}P$<0.05 timepoint vs. baseline, $^{\#\#}P$<0.01, timepoint vs. baseline, *N*=8-11. (**F**) Dynamic paintbrush responses of hemoglobin control and SCD FMT recipients throughout FMT paradigm; Fisher's exact post hoc comparisons: *P<0.05 control vs. SCD, **P<0.01, control vs. SCD, $^{\#}P$<0.05 timepoint vs. baseline, $^{\#\#}P$<0.01, timepoint vs. baseline, *N*=8-11. (**G**) Hindpaw withdrawal latency of male mice to radiant heat application at FMT timepoint; Mann-Whitney test *P=0.0286. (**H**) Hindpaw withdrawal latency of female mice to radiant heat application at FMT timepoint; Mann-Whitney test *P=0.0159. (**I**) Serum levels of FITC-dextran in control and SCD FMT recipients at FMT timepoint. (**J**) Colony forming units present on TSA III Blood Agar after plating homogenized mesenteric lymph node tissues from control and SCD FMT recipients at FMT timepoint. Relative abundance of the following genera in control and SCD FMT recipients at FMT timepoint: (**K**) *Enterorhabdus* and (**L**) *Roseburia;* LEfSe P<0.05, n.d.: not detected.

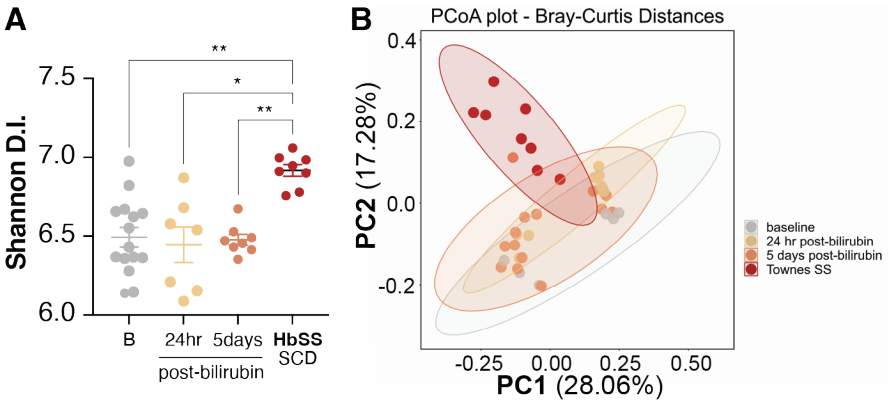

Figure S4: Oral bilirubin treatment alters gut microbiota, Related to Figure 4. (**A**) Alpha diversity of fecal material collected from hemoglobin control mice before and at various time points following oral bilirubin (200μM) administration as compared to SCD mice fecal material (Shannon diversity index, *P*=0.00123). (**B)** Beta diversity observed in fecal material collected from hemoglobin control mice before and at various time points following

	control FMT		SCD FMT	
	1X	***>1X***	***1X***	***>1X***
cell number	30	39	33	52
cell diameter (μm)	27.09 ± 0.62	25.72 ± 0.59	27.91 ± 0.65	27.08 ± 0.43
capacitance (pF)	37.50 ± 3.28	32.37 ± 2.23	34.28 ± 1.97	34.17 ± 2.23
RMP (mV) [a]	-66.16 ± 1.78	-62.56 ± 2.18	-67.00 ± 1.48	-60.74 ± 1.74
rheobase (pA) [a]	797.9 ± 99.46	240.5 ± 18.18	923.6 ± 93.82	283.4 ± 26.98
input resistance (mΩ) [a]	153.9 ± 25.04	369.8 ± 35.44	144.4 ± 26.35	372.2 ± 27.90
AP threshold (mV) [a]	-29.91 ± 1.25	-21.09 ± 1.26	-27.38 ± 1.61	-22.15 ± 0.89
AP amplitude (mV) [b]	64.12 ± 2.18	61.34 ± 1.47	61.05 ± 2.00	65.10 ± 1.11
AP half-width (ms) [a]	1.38 ± 0.09	1.73 ± 0.06	1.21 ± 0.07	1.80 ± 0.06

Table S1. Passive and active membrane properties of NJG neurons isolated from C57BL/6 mice 24 hours following SCD or control FMT, Related to Figure 2. Mean ± SEM listed for all properties. 2-way ANOVA main effect of fire type: [a]; 2-way ANOVA interaction between fire type x treatment: [b]; Bonferroni post-hoc tests: **P*<0.05, ***P*<0.01; 1x: fires only once, >1X: fires more than once, RMP: resting membrane potential, AP: action potential).

	vehicle		bilirubin	
	1X	***>1X***	***1X***	***>1X***
cell number	22	23	31	18
cell diameter (μm) [a,b]	21.63 ± 1.02*	18.71 ± 0.48*	19.03 ± 0.65	18.29 ± 0.72
capacitance (pF) [a]	50.22 ± 10.88	22.96 ± 2.08	35.62 ± 7.35	22.46 ± 2.68
RMP (mV) [a]	-62.14 ± 1.81	-56.78 ± 1.89	-59.61 ± 1.81	-56.94 ± 2.14
input resistance (mΩ) [a]	367.6 ± 81.67	756.5 ± 165.3	388.1 ± 56.18	860.5 ± 119.9
rheobase (pA) [a]	523.6 ± 130.0	82.61 ± 14.26	701.6 ± 212.0*	76.11 ± 12.34*
AP threshold (mV) [a]	-25.21 ± 3.46	-16.11 ± 2.55	-25.38 ± 2.04*	-13.46 ± 2.78*
AP amplitude (mV) [a]	75.96 ± 5.72	90.33 ± 3.37	67.76 ± 4.88**	92.22 ± 4.03**
AP half-width (ms)	2.97 ± 0.51	2.72 ± 0.28	3.28 ± 0.38	2.75 ± 0.30
spontaneous activity	4 of 23		4 of 18	

Table S2. Passive and active membrane properties of NJG neurons isolated from bilirubin (200 μM) or vehicle treated mice, Related to Figure 4. Mean ± SEM listed for all properties. 2-way ANOVA main effect of fire type: [a]; 2-way ANOVA main effect of treatment: [b]; Bonferroni post-hoc tests: **P*<0.05, ***P*<0.01 (groups being compared are indicated by matching symbols); 1X: fires only once, >1X: fires more than once, RMP: resting membrane potential, AP: action potential.

	Controls (*N*=25)	SCD patients (*N*=25)
Age (years; mean ± SD)	10.76 ± 3.49	12.84 ± 2.66
Gender: female	14 (56%)	13 (52%)
Genotype		
HbSS	N/A	17 (68%)
HbSC		6 (24%)
HbSβ+thal		1 (4%)
SO Arab		1 (4%)

Table S3. Participant demographics and clinical characteristics for metabolomic studies, Related to Figure 5.

	Related controls (*N*=53)	Unrelated controls (*N*=77)	SCD patients (*N*=138)
Age (years; mean ± SD)	28.71 ± 12.17	27.30 ± 16.87	16.24 ± 12.56
Gender: male	13 (25%)	22 (29%)	74 (54%)
Genotype			
HbSS	N/A		89 (64%)
HbSC			40 (29%)
HbSβ+thal			7 (5%)
HbSβ0-thal			2 (1%)

Table S4. Participant demographics and clinical characteristics for 16S sequencing studies, Related to Figure 5.

Donor ID	Age	Sex	Ethnicity	Cause of Death
26	77	F	White	Stroke/Fall
33	22	M	White	Head Trauma/Fall
343	69	F	White	Cerebral vascular accident/Stroke

Table S5. Human nodose ganglia donor demographics, Related to Figure 6.